Midbrain encodes sound detection behavior without auditory cortex

Tai-Ying Lee, Yves Weissenberger, Andrew J King, Johannes C Dahmen

Department of Physiology, Anatomy and Genetics, University of Oxford, Oxford, United Kingdom

Correspondence should be addressed to J.C.D. (johannes.dahmen@dpag.ox.ac.uk).

Abstract

Hearing involves analyzing the physical attributes of sounds and integrating the results of this analysis with other sensory, cognitive and motor variables in order to guide adaptive behavior. The auditory cortex is considered crucial for the integration of acoustic and contextual information and is thought to share the resulting representations with subcortical auditory structures via its vast descending projections. By imaging cellular activity in the corticorecipient shell of the inferior colliculus of mice engaged in a sound detection task, we show that the majority of neurons encode information beyond the physical attributes of the stimulus and that the animals' behavior can be decoded from the activity of those neurons with a high degree of accuracy. Surprisingly, this was also the case in mice in which auditory cortical input to the midbrain had been removed by bilateral cortical lesions. This illustrates that subcortical auditory structures have access to a wealth of non-acoustic information and can, independently of the auditory cortex, carry much richer neural representations than previously thought.

Introduction

Classically, perception is considered to rely on the flow of information from the sensory periphery via a sequence of hierarchically-organized brain structures up to the cortex. The ascending sensory pathways connecting these structures have been studied extensively and much has been learned about how signals are relayed, how features are extracted, and how information is integrated to produce increasingly abstract representations of the sensory environment. These pathways are paralleled by descending pathways that can feed information back to lower-order sensory structures. The fact that descending projections often outnumber their feedforward counterparts (Sherman, 2007) attests to their likely importance for brain function. This may include turning an otherwise passive, stimulus-driven device into an active and adaptive brain that is capable of processing sensory input within its behavioral context and, therefore, able to learn and create meaning (Engel et al., 2001; Kraus and White-Schwoch, 2015; Malmierca, Anderson and Antunes, 2015).

The descending projections of the auditory cortex target all major subcortical stations of the auditory pathway and are among the largest pathways of the brain (Winer, 2006; Bajo and King, 2013; Antunes and Malmierca, 2021), making them a particularly suitable system for investigating the behavioral and physiological consequences of corticofugal processing. One of their main targets is the inferior colliculus (IC), an obligatory midbrain relay for nearly all ascending auditory input. The corticocollicular projection primarily terminates in the non-lemniscal shell of the IC. The shell encapsulates and is extensively connected with the central nucleus of the IC, which forms part of the tonotopically organized core or lemniscal auditory pathway to the primary auditory cortex. The projection from the auditory cortex to the midbrain was identified almost a century ago (Mettler 1935) and decades of research have since demonstrated that manipulating the activity of descending projection neurons can alter the collicular representations of multiple sound features, influence adaptive plasticity and perceptual learning, and even trigger an innate flight response (Suga 2008; Nakamoto et al 2008; Bajo et al 2010; Xion et al 2015; Blackwell et al 2020). However, experimental evidence, especially from behaving animals, that could help explain what information the auditory midbrain and other subcortical sensory structures rely on their cortical input for is still very limited.

Interactions between different sensory pathways occur at multiple processing levels and they are also closely linked with the brain's motor centers and neuromodulatory regions. Indeed, recordings in awake animals have shown that behavior, cognition and brain state can strongly influence activity in the sensory pathways (Schneider and Mooney, 2018; McCormick et al., 2020; Parker et al., 2020). Consistent with a hierarchical view of sensory processing in which neurons at higher levels carry progressively more complex representations of the world, such contextual influences appear particularly strong in the cortex (Stringer et al,. 2019; Musall et al., 2019) and may to a large extent be the result of intracortical processing (Noudoost et al., 2010; Schneider et al., 2014; Song et al., 2017). Nevertheless, non-acoustic and contextual variables can also alter sensory processing at subcortical levels, including the IC and particularly its shell (Metzger et al., 2006; Gruters and Groh, 2012; Chen and Song, 2019; Yang et al., 2020; Parras et al., 2017; Saderi et al., 2021; Shaheen et al., 2021). This raises the possibility that these context-dependent effects may be inherited from the auditory cortex.

To test whether auditory midbrain neurons convey behaviorally-relevant signals that depend on descending cortical inputs, we imaged corticorecipient IC shell neurons in mice engaged in a sound detection task. We found that the activity of most neurons contained information beyond the physical attributes of the sound and that this information could be used to decode the animals' behavior with a high degree of accuracy. Surprisingly, this was the case both in

mice with an intact cortex and those in which the auditory cortex had been lesioned. These findings suggest that subcortical auditory structures have access to a wealth of non-auditory information independently of descending inputs from the auditory cortex. Consequently, the contextually-enriched representations that are characteristic of sensory cortices can arise from subcortical processing.

Results

Transient suppression of the auditory cortex impairs sound detection. Our aim was to characterize the activity of neurons in the shell of the IC in animals engaged in sound-guided behavior and assess how this activity is influenced by the input from the auditory cortex. To this end, we trained water-regulated mice on a sound detection task (Figure 1A) in which they were rewarded with a drop of water for licking in response to a click sound. Transient pharmacological silencing of auditory cortex using the GABA-A agonist muscimol has been shown to abolish the ability of rodents (Talwar et al., 2001), including head-fixed mice (Li et al., 2017), to perform a sound detection task, making this approach unsuitable for our aim of exploring the role of IC during behavior. We found that optogenetic suppression of cortical activity by photoactivating ChR2-expressing inhibitory neurons in *GAD2-IRES-cre* mice (Lohse et al., 2020) also significantly impaired sound detection performance (Figure 1B,C), albeit not to the same degree as pharmacological silencing. Although a control group in which the auditory cortex was injected with an EYFP virus lacking ChR2 would be required to confirm that the altered behavior results from an opsin-dependent perturbation of cortical activity, this result shows that this manipulation is also unsuitable for this study as it would leave us unable to determine whether any changes in the activity of IC neurons arise from removal of their auditory cortical input or are a consequence of alterations in the animals' behavior.

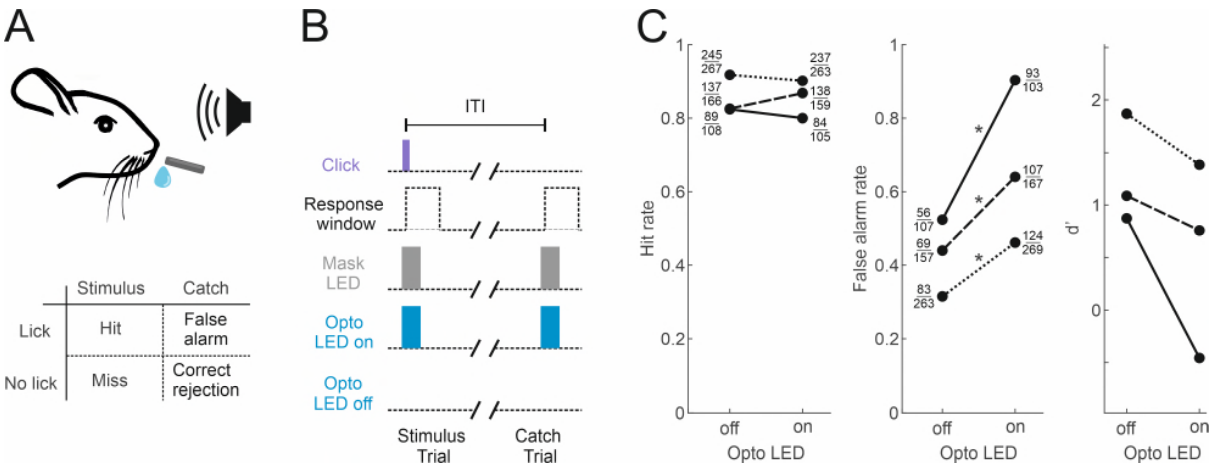

Figure 1. Optogenetic inactivation of auditory cortex impairs sound detection performance in head-fixed mice. (**A**) Schematic of the click detection task. (**B**) Trial structure for experiments involving optogenetic manipulation. Stimulus trials (click) and catch trials (no click) were randomly interleaved and consecutive trials separated by a randomly varying inter-trial interval (ITI). LEDs placed over each auditory cortex were switched on randomly in half of the stimulus and catch trials to photoactivate the opsin. A separate set of LEDs (Mask LEDs) placed directly in front of the mouse's eyes were switched on in all Opto-on and Opto-off trials to prevent mice from visually registering the light from the photoactivation LEDs. (**C**) Detection performance in trials during which light was shone on the auditory cortex for optogenetic silencing (Opto LED – on) vs control trials (Opto LED - off). Different line styles indicate different mice (n = 3). Numbers next to data points indicate numbers of hit and false alarm trials over total number of stimulus and catch trials, respectively. *: $p < 0.001$, two-sided Chi-squared proportion test.

Auditory cortex lesions leave detection ability intact. Several recent studies have shown that in contrast to the disruptive effects of transient silencing, cortical lesions leave performance in some sensory tasks intact (Hong et al., 2018; Ceballo et al., 2019; O'Sullivan et al., 2019). In order to assess how auditory cortex lesions impact sound detection performance, we therefore compared the performance of mice with bilateral lesions of the auditory cortex (n = 7) with non-lesioned controls (n = 9).

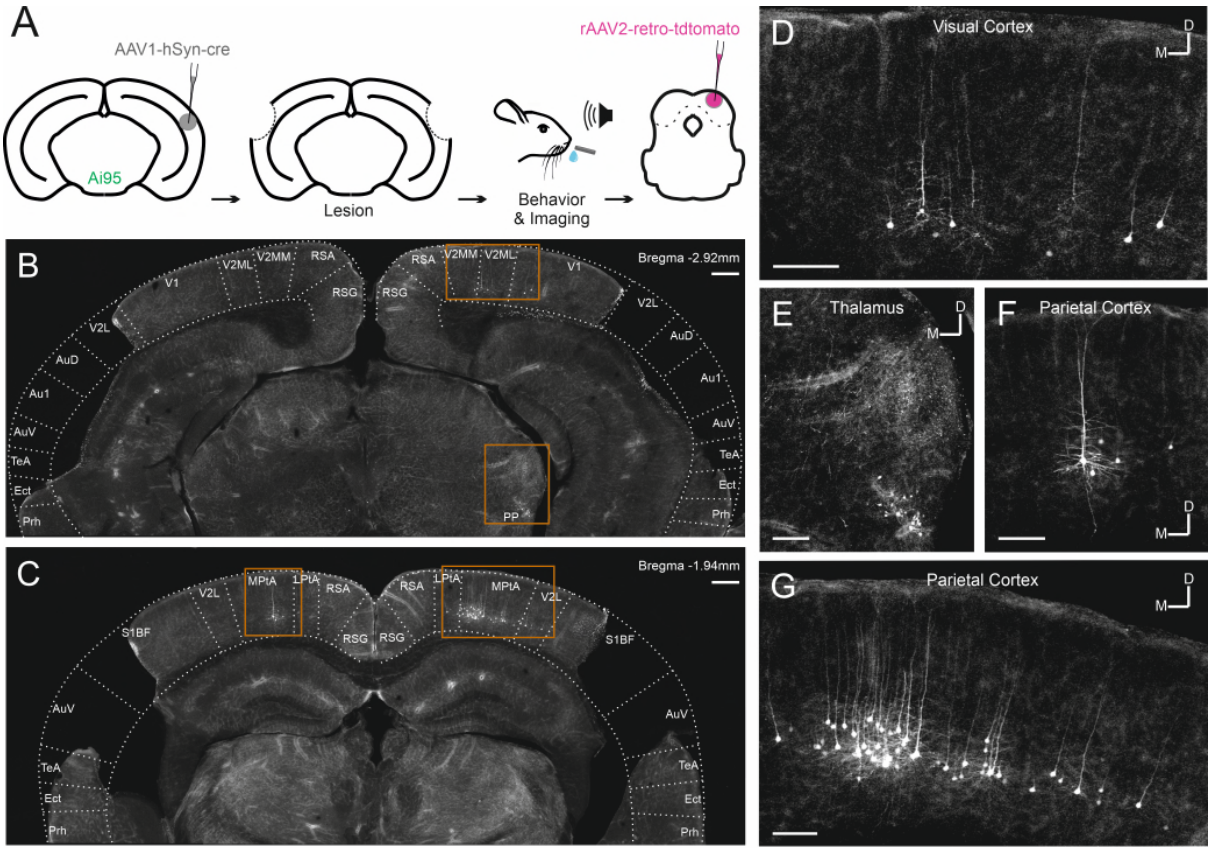

Figure 2. Retrograde viral tracing of IC-projecting neurons in bilaterally lesioned mice. (**A**) Timeline of experimental procedures. AAV1.hSyn.cre.WPRE was injected into the right auditory cortex of GCaMP6f reporter (Ai95D) mice. This causes transsynaptic delivery of the virus to the IC and expression of GCaMP6f in corticorecipient IC neurons. Several weeks later, the mice underwent bilateral lesioning of auditory cortex either by aspiration or by thermocoagulation (see Figure 2 - figure supplement 2 for histological sections from a mouse that underwent thermocoagulation) and were implanted with a glass window over the right auditory cortex. Following recovery from this procedure, water access was restricted and, 2-3 days later, behavioral training and imaging commenced. After data collection had been completed, rAAV2-retro-tdTomato was injected in the dorsal IC in order to label corticocollicular neurons that had remained intact. (**B**,**C**) Coronal sections showing lesion extent at different rostro-caudal positions for one example mouse. Area borders were drawn onto the images according to Paxinos and Franklin (2001). No retrogradely-labeled neurons were found near the lesion borders, suggesting that the auditory cortex had been completely removed. Corticocollicular projections from non-temporal regions as well as thalamocollicular projections remained intact. Scale bars, 200 µm. (**D**) High magnification image (location shown by the upper rectangle in **B**) showing corticocollicular neurons in visual cortex. Scale bar, 100 µm. (**E**) High magnification image (location shown by the lower rectangle in **B**) showing thalamocollicular neurons in the peripeduncular nucleus of the thalamus (PP). Scale bar, 100 µm. (**F,G)** High magnification images (locations shown by the left and right rectangles in **C**, respectively) showing corticocollicular neurons in the parietal cortex. Scale bars,100 µm. Cortical area abbreviations: Au1, primary auditory; AuD, secondary auditory, dorsal; AuV, secondary auditory, ventral; Ect, ectorhinal; LPta, lateral parietal association; MPta, medial parietal association; Prh, perirhinal; RSG, retrosplenial granular; RSA, retrosplenial agranular; S1BF, primary somatosensory, barrel field; TeA, temporal association; V1, primary visual; V2L, secondary visual, lateral; V2ML, secondary visual mediolateral; V2MM, secondary visual mediomedial.

Most corticocollicular neurons project ipsilaterally, with a substantial proportion also sending axons to the contralateral midbrain (Stebbings et al., 2014). The majority of corticocollicular neurons are found in the temporal cortex, and overwhelmingly in the auditory fields, while a small fraction populates adjacent areas, such as the temporal association area (Figure 2 - figure supplement 1). After the experiments, we injected a retrogradely-transported viral tracer (rAAV2-retro-tdTomato) into the right IC to determine whether any corticocollicular neurons remained after the auditory cortex lesions (Figure 2, Figure 2 – figure supplement 2, Figure 2 – figure supplement 3). The presence of retrogradely-labeled corticocollicular neurons in non-temporal cortical areas (Figure 2) was not the result of viral leakage from the dorsal IC injection sites into the superior colliculus (Figure 2 – figure supplement 3).

The ability of the mice to learn and perform the click detection task was evident in increasing hit rates and decreasing false alarm rates across training days (Figure 3A, $p < 0.01$, mixed-design ANOVAs). There was no difference between lesioned and non-lesioned mice in their learning speed (Figure 3A, $p > 0.05$, mixed-design ANOVAs) or psychometric functions (Figure 3B, $p > 0.05$, mixed-design ANOVA). Cortical lesioning thus leaves behavioral sensitivity to clicks intact and therefore provides a means of examining the effects of removing corticocollicular input, albeit non-reversibly, without directly affecting sound detection performance.

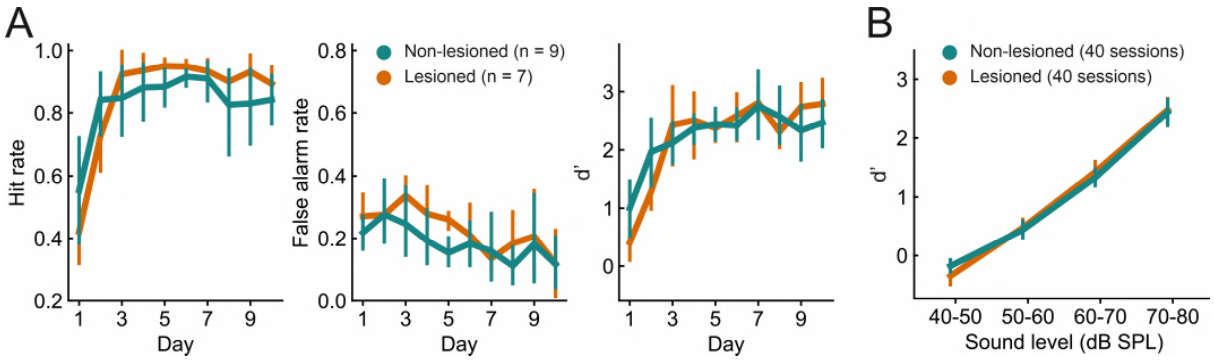

Figure 3. Lesioned and non-lesioned mice are indistinguishable in their click detection learning rate and sensitivity. (**A**) Hit rate, false alarm rate and d' over time for lesioned and non-lesioned animals. (**B**) d' as a function of sound level. The sound levels used were not identical across all mice and were therefore combined into 10-dB wide bins. Error bars indicate 95% confidence intervals.

Transsynaptic labeling and two-photon calcium imaging of auditory corticorecipient IC neurons. Manipulations of auditory cortical activity can influence the activity of neurons throughout the IC, including the central nucleus (Suga 2008, Nakamoto et al., 2008), where corticocollicular axons are relatively sparse (Stebbings et al 2014). The strongest effects, however, tend to be observed in the shell, where cortical input is densest (Nakamoto et al., 2008; Vila et al 2019; Blackwell et al., 2020). But even here, effects can be subtle (Vila et al., 2019) or undetectable (Blackwell et al., 2020), especially for cortical silencing. It is also unclear whether the IC neurons recorded in these studies receive cortical input or not. Therefore, we took a projection-specific approach to record the activity of IC neurons that receive direct input from the auditory cortex. More specifically, we injected AAV1.hSyn.Cre.WPRE, a virus with anterograde transsynaptic spread properties (Zingg et al., 2017), into the right auditory cortex of, initially, a tdTomato (Ai9) reporter mouse. This resulted in the expression of Cre recombinase and the reporter gene in neurons that receive input from the auditory cortex, including the corticorecipient neurons of the IC (Figure 4A). By employing this approach in GCaMP6f (Ai95D) reporter mice, we could target the expression of a calcium indicator to

corticorecipient IC neurons. We then proceeded to record the activity of corticorecipient neurons within about 150 µm of the dorsal surface of the IC using two-photon microscopy (Figure 4B, Video 1).

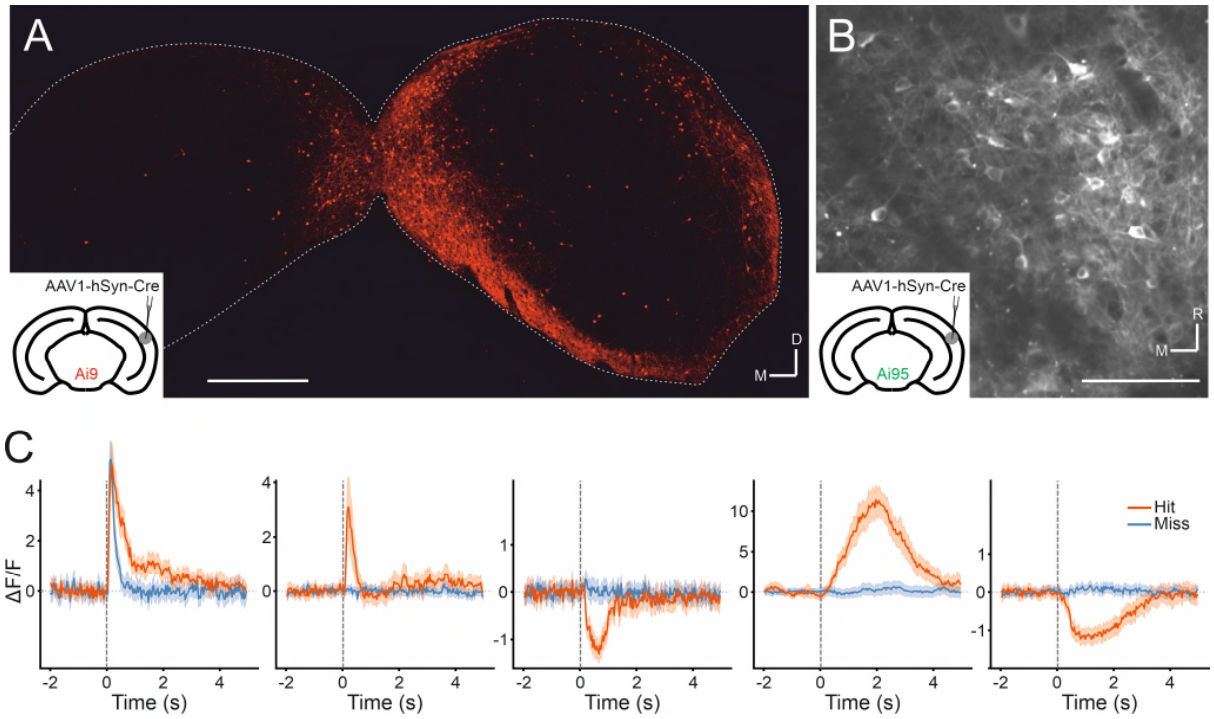

Figure 4. Transsynaptic targeting and two-photon calcium imaging of corticorecipient IC shell neurons. (**A**) Coronal section of the left and right IC of a tdTomato-reporter (Ai9) mouse in which AAV1.hSyn.Cre.WPRE had been injected into the right auditory cortex three weeks before perfusion. The transsynaptically transported virus drove expression of Cre recombinase and tdTomato in neurons that receive input from the auditory cortex, including the corticorecipient neurons in the IC. tdTomato-labeled neurons were predominantly found in the shell of the ipsilateral (right) IC. Scale bar, 500 µm. (**B**) In vivo two-photon micrograph taken approximately 100 µm below the dorsal surface of the right IC of a GCaMP6f-reporter mouse (Ai95D) in which GCaMP6f expression had been driven in corticorecipient IC neurons by injection of AAV1.hSyn.Cre.WPRE into the right auditory cortex. See Video 1 for corresponding video recording. Scale bar, 100 µm. (**C**) Example average response profiles of five corticorecipient IC neurons for different trial outcomes. Vertical line at time 0 s indicates time of click presentation. Shaded areas represent 95% confidence intervals.

Corticorecipient IC neurons display heterogeneous response profiles. The activity of individual corticorecipient IC neurons showed distinct response profiles across neurons and trial outcomes (hit vs miss) (Figure 4C). While averaging across all neurons cannot capture the diversity of responses, the averaged response profiles suggest that it is mostly trial outcome rather than the acoustic stimulus and neuronal sensitivity to sound level that shapes those responses (Figure 4 – figure supplement 1). Indeed, close to half (1272 / 2649) of all neurons showed a statistically significant difference in response magnitude between hit and miss trials, while only a small fraction (97 / 2649) exhibited a significant response to the sound. While the number of sound-responsive neurons is low, it is not necessarily surprising given the moderate intensity and very short duration of the stimuli. For comparison: Using the same transgenics, labeling approach and imaging setup and presenting 200-ms long pure tones at 60 dB SPL with frequencies between 2 kHz and 64 kHz, we typically find that between a quarter and a third of neurons in a given imaging area exhibit a statistically significant response (data not shown).

To capture the heterogeneity of response patterns across all recorded neurons, we used an unsupervised clustering algorithm (Namboodiri et al. 2019) to group the average responses on hit and miss trials for each neuron. This yielded 10 clusters that displayed different response patterns over the course of the trial (Figure 5A, B). Most of the clusters exhibited distinct activity for hit vs miss trials. Some hit trial profiles were characterized by increases or decreases in activity, with a very sharp, short-latency onset, as in clusters 4 and 10 (see Figure 5 - figure supplement 1 for a scaled version of cluster 10), and others by much more gradual changes in which a peak occurred seconds after the trial onset, as in clusters 5 and 9. Cluster 3, which contained the smallest number of neurons, was an exception in that it showed a transient, short latency response to the stimulus for both trial outcomes. The response profiles of some other clusters, especially clusters 6 and 8, were also qualitatively similar across hit and miss trials and/or only weakly modulated across both trial types.

This suggests that the activity of the majority of neurons in the recorded population contained information beyond the physical properties of the stimulus. Given that licking causes self-generated sounds, IC neurons could, in principle, respond to the sound of licking. However, given how quiet these are - estimated to be just 12 dB SPL (Singla et al., 2017) - and that much of the response to such lick-related sounds is already canceled out at the level of the cochlear nucleus (Singla et al., 2017; but see Shaheen et al., 2021), it is highly unlikely that lick-related sounds play a major role in driving activity in the IC.

To assess whether certain response profiles depended on auditory cortical input, we compared the ratio of neurons from lesioned vs non-lesioned mice in each cluster to that of the overall recorded population. The number of recorded neurons was unequal for lesioned and non-lesioned mice (952 vs 1697, respectively), reflecting the fact that a greater proportion of imaging sessions in non-lesioned animals were carried out using a larger field of view, which contained larger numbers of neurons (Figure 5 - figure supplement 2). To account for this, the percentages shown on the pie charts were normalized to the ratio in the overall population (Figure 5C). Neurons from both groups were well represented across all 10 clusters and while a significant difference in the lesioned/non-lesioned ratio was found for four clusters, the difference between the groups was greater than 20% for only one of them. Furthermore, there was a close correspondence between the cluster averages of lesioned and non-lesioned mice (Figure 5 – figure supplement 3). This suggests that the IC shell can produce very similar output regardless of whether auditory cortical input is available or not.

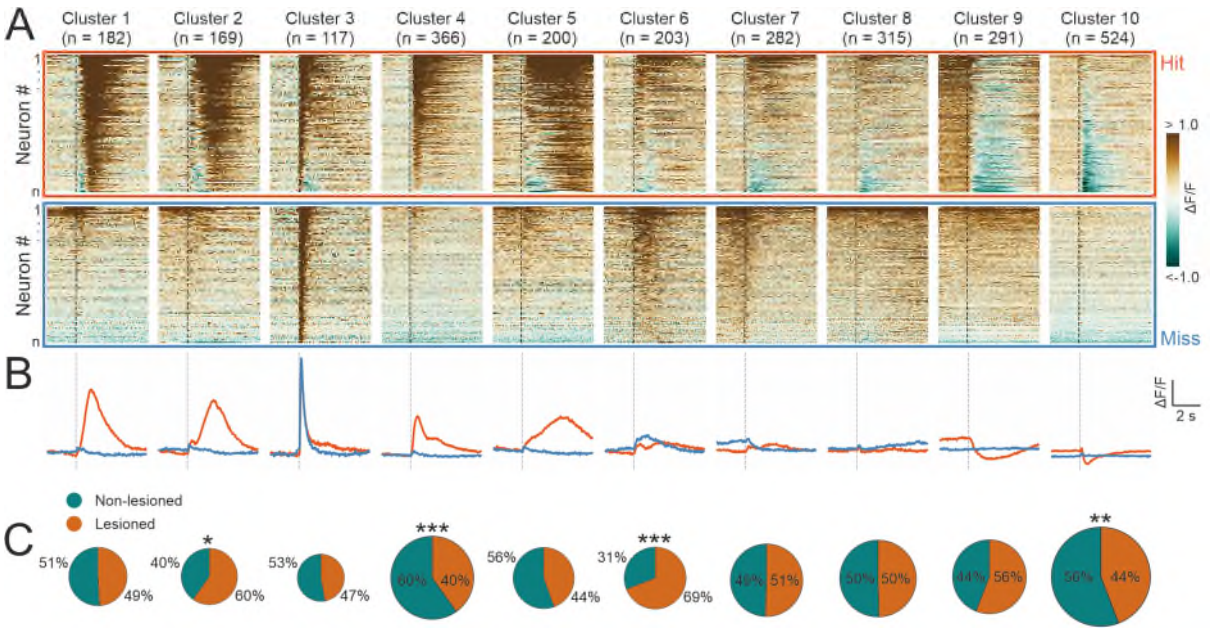

Figure 5. Corticorecipient IC neurons display heterogeneous response profiles. (**A**) Peri-stimulus time histograms for all neurons in the dataset separated by cluster identity: hit trials (top) vs miss trials (bottom). (**B**) Averaged response profiles obtained by taking the mean across all neurons in a cluster separately for hit (red) and miss (blue) trials. (**C**) Pie charts illustrating the proportion of neurons from lesioned and non-lesioned mice in each cluster. The size of each pie chart is proportional to the total number of neurons in each cluster. Given the unequal number of neurons from lesioned (952 neurons) and non-lesioned (1697 neurons) mice, the pie charts were normalized to the overall sample size such that a 50/50 split indicates a lesioned/non-lesioned distribution that is identical to that of the overall population. Asterisks indicate a significant difference between the lesioned/non-lesioned distribution in the given cluster and that in the overall population. *: $p < 0.05$, **: < 0.01, ***: $p < 0.001$, two-sided one proportion Z-test.

Behavior can be accurately decoded from neural activity in lesioned and non-lesioned mice. The average responses of individual neurons in the IC shell exhibited a variety of activity patterns associated with both the stimulus and the trial outcome (Figure 5A,B). To gain insight into how these activity patterns can be read out collectively on a trial-by-trial basis, we assessed the relationship between the trial-by-trial network activity and the trial outcome. We trained logistic regression models to classify hit vs miss trials on a trial-by-trial, frame-by-frame basis. As different populations of neurons were recorded in different imaging sessions, the models were trained separately for each session. “Dummy models”, which randomly classified trials while taking into account the probability of hit vs miss trials in a given session, were used as the baseline model performance. If the population activity of the IC shell contained information about the trial outcome, the performance of the models would be significantly above baseline.

In both lesioned and non-lesioned mice, the average model performance was significantly above baseline in classifying hit vs miss trials ($p < 0.05$, one-sided Wilcoxon signed-rank test or paired t-test with Bonferroni correction, Figure 6A), showed a temporal profile that is consistent with the dynamics of the activity profiles of some of the clusters, in particular clusters 1, 2, 4, 5, 9, 10 (Figure 5A,B), and was not meaningfully affected by differences in sound level distributions between hit and miss trials (Figure 6 – figure supplement 1) Additionally, the model performance in non-lesioned mice was significantly better than that in lesioned mice ($p < 0.05$, one-sided Mann-Whitney U test or t-test with Bonferroni correction, Figure 6A). The difference in the decoding performance was not the result of the difference in the number of neurons between non-lesioned and lesioned mice (Figure 6 - figure supplement 2).

By examining the corticocollicular labeling and referencing the histological sections against a mouse brain atlas (Paxinos and Franklin, 2001), we categorized the mice according to lesion size. Four of the seven lesioned animals had "(near-)complete" lesions, meaning that all (Figure 2) or an estimated ~95% (Figure 2 - figure supplement 2) of the auditory cortex had been lesioned, while the remaining mice had "partial" lesions, with an estimated 15% - 25% of the auditory cortex left intact. To assess whether the size of the lesions impacted the decoding performance, we compared the model performance between mice that had (near-)complete lesions and mice that had partial lesions. This revealed that the average decoding performance for mice with (near-)complete lesions was significantly better than that measured for mice with partial lesions. While this pattern of results may be unexpected, it is consistent with work showing smaller lesions being associated with greater somatosensory processing deficits (Hong et al., 2018). Additionally, the decoding performance in mice with (near-)complete lesions was largely indistinguishable from that in mice with an intact auditory cortex. Although the proportion of individual neurons with distinct response magnitudes in hit and miss trials in lesioned mice did not differ from that in non-lesioned mice, it was significantly lower when separating out mice with partial lesions (Figure 6 – figure supplement 3). These results imply that the activity of IC shell neurons can contain similar amounts of information about the animal's behavior regardless of whether descending input from the cortex is available or not (Figure 6B).

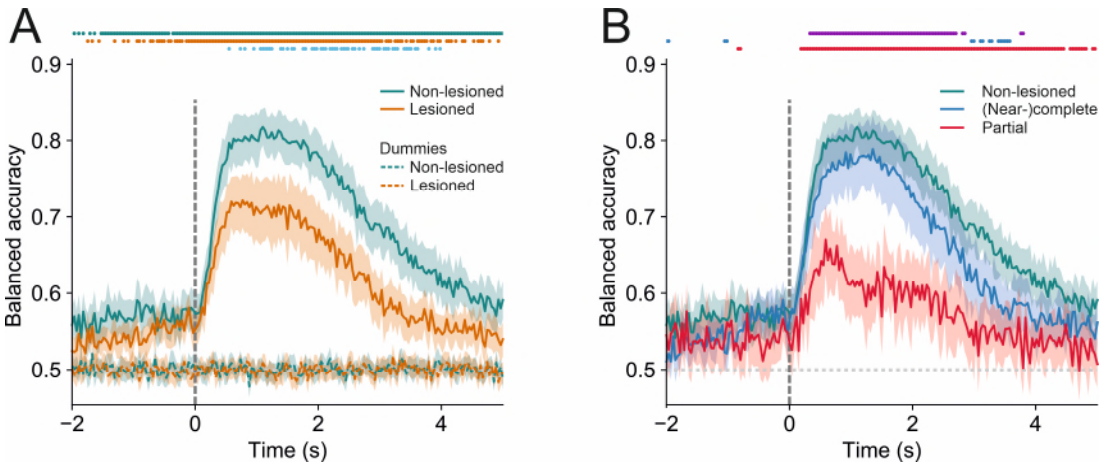

Figure 6. Trial outcome can be accurately decoded from neural activity in lesioned and non-lesioned mice. (**A**) Average decoding accuracy of logistic regression models as a function of time against dummy models with a score of 0.5 meaning chance performance and a score of 1 being the maximum. Data shown depict the mean model accuracy across 37 (lesioned) and 38 (non-lesioned) sessions, respectively. Dots at the top indicate the timepoints (frames) where the model performance was significantly different between trained and dummy models for non-lesioned mice (teal) or lesioned mice (orange) ($p < 0.05$, one-sided Wilcoxon signed-rank test or paired t-test with Bonferroni correction, depending on whether normality assumption was met), and between the trained models for non-lesioned vs lesioned mice (blue) ($p < 0.05$, one-sided Mann-Whitney U test or t-test with Bonferroni correction, depending on whether normality assumption was met). (**B**) Same as **A** but the average model accuracy is plotted separately for mice with (near-)complete and partial lesions. Dots at the top indicate the timepoints where the model performance was significantly different between partial vs (near-)complete mice (purple), (near-)complete vs non-lesioned mice (blue), and partial vs non-lesioned mice (red) ($p < 0.05$, one-sided Mann-Whitney U test or t-test with Bonferroni correction, depending on whether normality assumption was met). Shaded areas represent 95% confidence intervals.

Pre-stimulus activity is predictive of the upcoming trial outcome. Remarkably, decoding accuracy was better than baseline even before stimulus onset. This could reflect changes in the network state that led or contributed to the upcoming trial outcome. For instance, changes

in arousal or motivation can alter both the probability that an upcoming stimulus is detected and the activity of neurons in the network (Lee and Dan, 2012, McGinley et al., 2015). The decoding models might detect such changes in activity, resulting in higher decoding accuracy prior to stimulus onset. Additionally, pre-stimulus differences in hit and miss trial activity could also reflect the anticipation of an upcoming stimulus (Ruth et al., 1974; Nienhuis and Olds, 1978; Metzger et al., 2006) and the resulting change in attentional state. Inter-trial intervals in our experiments were randomly drawn from a normal distribution with a mean and standard deviation of 8 s and 2 s, respectively, and a lower bound of 3 s. Nevertheless, spontaneous licks did not occur at random times during the peri-catch trial periods following hit trials. Instead, average lick rates approximated the inter-trial interval distribution (Figure 6 - figure supplement 4A-D), suggesting that mice learned to adapt their behavior to this distribution and anticipate the timing of upcoming stimuli (Figure 6 - figure supplement 4E,F). Assuming that successfully anticipating the timing of an upcoming stimulus confers a greater chance of detecting the stimulus, neurons whose activity reflects that anticipation might be expected to show differences in pre-trial activity between hit and miss trials that could be detected by a decoding model. Note that for the analysis illustrated in Figures 5 and 6, hit trials were excluded if there were any licks between -500 ms and +120 ms (the latter number representing the lower bound of the animals' lick-latency) relative to stimulus onset, suggesting that changes in pre-stimulus activity cannot be directly related to licking.

Discussion

Imaging auditory corticorecipient neurons in the dorsal shell of the IC in mice trained to perform a sound detection task revealed that the majority of neurons exhibited distinct activity profiles for hit and miss trials, implying that they encode information beyond just the physical attributes of the stimulus. Indeed, using logistic regression models to classify hit vs miss trials, we found that the animals' behavioral choice can be read out from these neurons with a high degree of accuracy. Importantly, the difference in IC activity between hit and miss trials was observed across different sound levels and was not due to a difference in the sound level distribution for these two trial outcomes. Surprisingly, neural activity profiles and the decoding performance were similar in mice in which the auditory cortex had been lesioned bilaterally, suggesting that the midbrain has, independently of the auditory cortex, access to a wealth of non-acoustic information, which may be sufficient to support sound detection behavior.

Auditory corticocollicular axons terminate predominantly in the shell of the IC (Stebbings et al., 2014; Bajo and King, 2013) and the strongest effects of cortical manipulations have been reported in this region (Nakamoto et al., 2008; Vila et al 2019; Blackwell et al., 2020). However, these effects can be subtle (Cruces-Solis et al., 2018; Vila et al., 2019) or undetectable, especially when optogenetic silencing is used (Blackwell et al., 2020). Because of this and uncertainties over exactly what proportion of neurons in the shell of the IC is innervated by the auditory cortex and even where the border lies with the underlying central nucleus (Barnstedt et al., 2015), we used an anterograde transsynaptic tagging approach (Zingg et al., 2017) to identify corticorecipient neurons. This therefore maximized the chances of revealing the contribution of descending cortical input to the response properties of these midbrain neurons. We imaged across the optically accessible dorsal surface of the IC down to a depth of about 150 µm below the surface. Consequently, the neurons we recorded were located predominantly in the dorsal cortex. However, identifying the borders between different subdivisions of the IC is not straightforward and we cannot rule out the possibility that some were located in the lateral cortex.

Inferior colliculus neurons exhibit task-related activity

Our recordings from corticorecipient neurons in the IC are consistent with previous studies demonstrating that neural representations of behavioral variables can be found in the auditory midbrain (Ruth et al., 1974; Nienhuis and Olds, 1978; Metzger et al., 2006; Gruters and Groh, 2012; Chen and Song, 2019; Yang et al., 2020; Saderi et al., 2021, Franceschi and Barkat, 2021; Shaheen et al., 2021; Quass et al., 2023). In keeping with responses recorded in the auditory cortex (Francis et al., 2018; Franceschi et al., 2021) and IC (Chen and Song 2019; Yang et al., 2020; Franceschi et al., 2021) of behaving mice, we found that the activity of most neurons was facilitated and about a third were suppressed during the sound detection task. Overall, only a small minority of clusters (mostly cluster 3) in our dataset showed what could be characterized as largely behavior-invariant response profiles to the auditory stimulus. In contrast, a large number of neurons were clearly driven by variables other than the stimulus itself. Their activity may represent the choice (to lick or not to lick) that an animal made, preparatory motor activity, corollary discharge or the reward and the somatosensory or gustatory feedback associated with its consumption, as well as modulation by the animal's cognitive and behavioral state. Due to the task structure used, for the most part, it was not possible to unambiguously assign activity profiles to a particular variable. Nevertheless, we can speculate that neurons with late transients, such as in cluster 5, are more likely to represent corollary discharge and signals associated with the consumption of the reward, while those with very short latency peaks, as in clusters 4 and 10, may represent the animals' choice and/or preparatory motor activity.

When engaged in the detection task, an animal's arousal or motivational state may vary spontaneously or as a result of changes in, for instance, thirst, time of day or time into a session. In addition, cognitive factors, such as expectations about the timing of an upcoming trial (Ruth et al., 1974; Nienhuis and Olds, 1978; Metzger et al., 2006), which mice may have derived by learning the shape of the inter-trial interval distribution, may lead to variations in arousal or attentional state. Pre-trial differences in activity as well as the above-chance decoding performance before trial onset likely reflect the joint impact of those state changes on the activity of IC corticorecipient neurons and detection sensitivity (McCormick et al., 2020).

Contribution of the auditory cortex to task-related activity in the midbrain

Given the massive corticofugal projections that exist within the auditory system (Bajo and King, 2013), we hypothesized that task-related activity in the IC might depend on descending inputs from the auditory cortex. To address this, we imaged corticorecipient IC neurons during the same sound detection task after removing the cortical input. Consistent with previous work in the auditory (O'Sullivan et al., 2019) and somatosensory systems (Hong et al., 2018), we found that transient optogenetic silencing of the auditory cortex impaired sound detection, whereas cortical lesions had no effect on detection behavior, with lesioned mice learning the task as quickly as non-lesioned animals and achieving the same level of performance. In order to determine whether the absence of auditory cortical input alters the activity of IC neurons during sound detection behavior, we therefore focused on mice with bilateral cortical lesions to avoid the potentially confounding effects that reduced detection sensitivity produced by transient cortical silencing might have on the activity of IC neurons. For the same reason, we opted against the more targeted approach of optogenetic silencing of corticocollicular axons. Furthermore, it would have been difficult to silence the entire corticocollicular projection and the higher light powers required for manipulating axons compared to somata would have risked transmitting light to the cortex or other corticofugal targets, potentially causing behavioral changes and/or sacrificing specificity. Locally silencing corticocollicular axons

would also have left indirect transmission via the thalamus between the auditory cortex and IC intact and would have been very challenging to verify. Finally, it has been reported that using optogenetic silencing tools in axons can have unintended consequences (Wiegert et al., 2017).

In keeping with our findings, numerous studies (reviewed in e.g. Pickles, 1988; Buser and Imbert, 1992) have shown that simple auditory skills, including the ability of freely moving rats to detect sounds (Kelly, 1970), are unaffected by the removal of the auditory cortex. However, transient pharmacological silencing of the auditory cortex in freely moving rats (Talwar et al., 2001), as well as head-fixed mice (Li et al., 2017), completely abolishes sound detection (but see Gimenez et al., 2015). The time course of the effects produced by muscimol application (Talwar et al 2001) suggests that there is a relationship between the size of the behavioral deficit and the degree of cortical inactivation. Consequently, milder impairments may be produced by the optogenetic approaches employed by us and others (Kato et al 2015; O'Sullivan et al., 2019) because of incomplete suppression of cortical activity. Alternatively, the larger behavioral effects reported following muscimol application may be due to diffusion of the drug to other brain structures, potentially including the IC. Although our results cannot speak directly to the question of whether the preservation of sound detection without auditory cortex reflects a rewiring or repurposing of circuits in the brain, this seems unlikely given that other studies have shown that trained mice achieve pre-lesion performance levels on simple auditory discrimination (Ceballo et al., 2019; O'Sullivan et al., 2019) or somatosensory detection (Hong et al., 2018) tasks suddenly and within 48 hours following cortical ablation.

Why then does transient inactivation produce behavioral deficits? One possibility is that disabling the auditory cortex impacts behavior not because it contributes necessary computations or information, but because of the sudden and disruptive removal of tonic excitation (Oberle et al., 2021) to downstream targets (Otchy et al., 2015) that are indispensable for successful sound detection. In this scenario, normal operation would resume once synaptic scaling (Keck et al., 2013) had homeostatically restored normal activity in these structures, a process that has been suggested to take up to 48 hours and is consistent with the time course of recovery after lesions (Ceballo et al., 2019; Hong et al., 2018). Alternatively, several circuits may redundantly support sound detection. Silencing the auditory cortex might then transiently impede sound detection until the relevant downstream decision and motor structures have updated their synaptic weights and/or processing has shifted to the other circuits. Two observations, however, argue against this possibility. First, removing one of several redundant structures should leave some residual function intact and not have the devastating effect that pharmacological cortical silencing achieves (Talwar et al., 2001, Li et a., 2017). Second, other circuits mediating the acousticomotor transformation required for successful sound detection behavior very likely incorporate subcortical auditory structures, including the auditory midbrain. Activity in the IC may trigger actions (Cassedey and Covey, 1996), such as licking, via its direct projections to the superior colliculus, pontine nuclei and the periaqueductal gray (Hufman and Henson, 1990, Wenstrup et al., 1994, Casseday and Covey, 1996; Xiong et al., 2015) or indirectly via its projections to the auditory thalamus. If cortical lesioning results in a greater weight being placed on the activity in spared subcortical circuits for perceptual judgements, we would expect the accuracy with which trial-by-trial outcomes could be read out from IC neurons to be greater in mice without auditory cortex. However, that was not the case. This could imply that, following cortical lesions, greater weight is placed on structures other than the IC, with the thalamus being an obvious candidate, or that the auditory midbrain, thalamus and cortex are bypassed entirely if simple acousticomotor transformations, such as licking a spout in response to a sound, are handled by circuits linking

the auditory brainstem and motor thalamus via pedunculopontine and midbrain reticular nuclei (Inagaki et al., 2022).

Some differences were observed for mice with only partial lesions of the auditory cortex. Those mice had a lower proportion of neurons with distinct response magnitudes in hit and miss trials than mice with (near-)complete lesions. Furthermore, trial outcomes could be read out with lower accuracy from these mice. While this finding is somewhat counterintuitive and is based on only three mice with partial lesions, it has been observed before that smaller lesions can have a more disruptive effect than larger, more complete lesions, in that the time it takes mice to learn a whisker-dependent sensory detection task is anticorrelated with the size of their somatosensory cortex lesion (Hong et al., 2018). While the complete destruction of a cortical area severs all its communication with downstream structures, a partial lesion may actually be more disruptive by eradicating normal local processing while at the same time leaving intact some tissue, especially in the deeper output layers, which continues to transmit what are now aberrant activity patterns. The difference in decoding accuracy that we observed in the IC could thus be a consequence of residual and now disruptive cortical input.

Our results show that behavioral variables are encoded by corticorecipient neurons in the dorsal shell of the IC independently of their main source of descending input, the auditory cortex. It therefore seems likely that this region of the auditory midbrain is part of the circuit that supports sound detection behavior in the absence of the auditory cortex. Nevertheless, except for the regions immediately bordering the auditory cortex, corticocollicular neurons located in other areas were left intact. These relatively sparse descending projections to the IC, such as those originating from somatosensory cortical areas (Lohse et al., 2021; Lesicko et al., 2016) and parietal cortex may have contributed to the response profiles that we observed. Additional non-acoustic sensory input can reach the IC via brainstem nuclei (Lesicko et al., 2016; Shore and Zhou, 2006) and the superior colliculus (Chen et al., 2020; Coleman and Clerici, 1987). The latter, together with input from the substantia nigra (Olazabal and Moore, 1989) and the globus pallidus (Morizumi and Hattori, 1991) may also be a source of motor signals, while state changes may impact on the IC via inputs from neuromodulatory structures, including the locus coeruleus and the subparafascicular, dorsal raphe and tegmental nuclei (Chen et al., 2020, Liu et al., 2023).

Conclusion

Behavior is a major determinant of activity in the non-lemniscal auditory midbrain and thus key to understanding how it contributes to hearing. The anatomical feature that defines this structure more than any others is its connection with the auditory cortex. While modulation of IC activity by this descending projection has been implicated in various functions, most notably in the plasticity of auditory processing, we have shown in mice performing a sound detection task that IC neurons show task-related activity in the absence of auditory cortical input. These results therefore emphasize more than ever the need to factor in subcortical processing when considering how the cortex contributes to sound-guided behavior.

Materials and methods

Animals. All experiments were approved by the Committee on Animal Care and Ethical Review at the University of Oxford and were licensed by the UK Home Office (Animal Scientific Procedures Act, 1986, amended in 2012). We used 22 (3 female, 19 male) Ai95 (RCL-

GCaMP6f)-D (JAX 024105, Jackson Laboratories, USA), three (one female, two male) Gad2-IRES-Cre (JAX 010802, Jackson Laboratories, USA), six female Ai9 (RCL-tdT) (JAX 007909, Jackson Laboratories, USA), two female Ai95 (RCL-GCaMP6f)-D X VGAT-cre (JAX 016962, Jackson Laboratories, USA), three female Ai95 (RCL-GCaMP6f)-D X T29-1 (Camk2a-cre, JAX 005359, Jackson Laboratories, USA) and three (one male, two female) C57BL6/NTac.Cdh23 (MRC Harwell, UK) mice. All mice were 9–15 weeks old during data collection. They were maintained on a 12-h light/dark cycle and were housed at 20–24°C with a relative humidity of 45–65%.

Surgeries. For all surgical procedures, mice were premedicated with intraperitoneal injections of dexamethasone (Dexadreson, 4 mg), atropine (Atrocare, 1 mg) and carprofen (Rimadyl, 0.15 mg) before being anesthetized with isoflurane (1.5-2%) and administered with buprenorphine (Vetergesic, 1 ml/kg) postoperatively. Mice were then placed in a stereotaxic frame (Model 900LS, David Kopf Instruments, CA, USA) and their body temperature was kept constant at 37°C by the use of a heating mat and a DC temperature controller in conjunction with a temperature probe (FHC, ME, USA).

For injections in the auditory cortex of AAV1.hSyn.Cre.WPRE (Penn Vector Core), the skin over this part of the brain was shaved and an incision was made, after which three small holes were drilled (Foredom K.1070, Blackstone Industries, CT, USA) into the skull with a 0.4 mm drill bit and the virus injected using a pulled glass pipette and a custom pressure injection system. In order to express GCaMP6f or tdTomato in IC neurons that receive auditory cortical inputs, a total of 150-200 nl of AAV1.hSyn.Cre.WPRE was injected at three sites in the right auditory cortex of GCaMP6f (Ai95D) or tdTomato (Ai9) reporter mice, respectively, at depths of 450-550 µm below the brain surface. Given the anterograde transsynaptic spread properties of AAV1 (Zingg et al. 2017), this caused the expression of the desired fluorescent protein in structures that the auditory cortex projects to, including the shell of the IC (Figure 4A,B).

In order to prepare GAD2-Ires-Cre mice for the optogenetics experiments, we removed a large flap of skin over the parietal and temporal bones, partially removed the temporal muscles and performed a circular craniotomy of 3 mm diameter over each auditory cortex. We then injected a total of 500 nl of AAV5-EF1a-DIO-hChR2-EYFP, UNC Vector Core) bilaterally across 4 sites and two depths (200 and 600 µm) into the auditory cortex. Each craniotomy was covered with a circular 3 mm glass window that was attached to the edges of the skull with cyanoacrylate glue (Pattex Ultra Gel, Henkel), and the exposed skull was sealed with dental acrylic (C&B Superbond, Sun Medical, Japan) into which a custom steel bar was embedded for head fixation. Experiments commenced approximately three weeks afterwards.

The IC window implantation and cortical lesioning in the Ai95D mice were performed at least three weeks after the injections. The window implantation involved removing a flap of skin over the (inter-)parietal and occipital bone and making a circular 3 mm craniotomy over the midbrain. A 3-mm diameter glass coverslip that had been glued to a ~1 mm tall steel cylinder with 0.5 mm wall thickness was inserted into this craniotomy. The cylinder allowed us to press the glass window gently onto the brain (in order to minimize brain movement during experiments) and was then glued to the edges of the skull. For head fixation, we embedded a custom steel plate in the dental acrylic used to seal the exposed bone.

Lesions were performed as part of the cranial window implantation surgery. In those mice undergoing lesions, we removed a slightly larger flap of skin on both sides in order to expose the temporal bone, detached and deflected and/or partly removed the temporal muscle and then made, on both sides, an elliptical craniotomy over the auditory cortex of ~3 mm (dorsoventral) by 4 mm (rostrocaudal). The exposed tissue was then aspirated (Hong et al ., 2018) with a blunted 19 G needle connected to a suction pump (Eschmann Vp25, UK) or destroyed by thermocoagulation (Ceballo et al., 2019) with a cauterizer (Small Vessel Cauterizer Kit, FST, Germany) and the piece of skull that had been removed for the craniotomy was glued (Pattex Ultra Gel) back in place. In some of the lesioned mice, after completion of the imaging, 150 nl of a retrograde viral construct (rAAV2-CAG-tdTomato, UNC Vector Core) was injected into the dorsal IC across two to three sites at depths of 100-400 µm below the brain surface in order to visualize the remaining IC-projecting cortical neurons. The extent of the lesions was estimated from the histological sections and by referencing them against sections from a mouse brain atlas (Paxinos and Franklin, 2001). The experimenters were not blinded to the treatment group, i.e. lesioned or non-lesioned, but they were blind to the lesion size both during the behavior experiments and most of the data processing.

In order to visualize the distribution of IC-projecting neurons in mice without cortical lesions, 150 nl of the retrograde rAAV2-CAG-cre (UNC Vector Core) construct was injected into the dorsal IC of one Ai9 mouse with an intact cortex across three sites at depths of 100-400 µm below the brain surface.

Histology. For histological processing, mice were perfused transcardially, first with phosphate buffered saline (PBS) and then with 4% paraformaldehyde in (PBS), and their brains were sectioned coronally (100 µm thick) with a vibratome (Leica). Images were taken manually using a Leica DMR microscope, a confocal laser scanning microscope (Olympus FV1000) or with an automated slide scanner (Zeiss Axioscan Z1). The brain of one mouse (Figure 2 - figure supplement 1) was sectioned and imaged on a custom-built two-photon whole brain tomograph.

Click detection task. Starting 2-3 days before training commenced, the mice were habituated to head fixation in the experimental setup and their access to water was restricted to about ~1 ml per day, bringing their body weight down to about ~85% of the pre-restriction values. During the training phase, the mice were required to report a 0.5 ms broadband click stimulus of 80 dB SPL by licking a waterspout positioned in front of them. Licking within a 1.5-second response window (occasionally this was reduced in duration to discourage excessive licking) triggered an immediate water reward (~2 µl). Stimulus trials and catch (no stimulus) trials were randomly interleaved with an inter-trial interval drawn from a normal distribution with a mean and standard deviation of 8 s and 2 s, respectively, and a lower bound of 3 s. Successful reporting of the sound within the response window was scored a ‘hit’, while failure to respond was scored a ‘miss’. During catch trials, neither licking (‘false alarm’) during the 1.5-second response window nor withholding licking (‘correct rejection’) triggered a reward. To help the mice form an association between sound and reward, they received occasional ‘free’ rewards in stimulus trials during the initial training even when no licking occurred.

Once the mice had achieved a stable level of performance (typically two days with d’ > 1.5), quieter stimuli (41-71 dB SPL) were introduced. The range of sound levels was adjusted to each animal’s behavioral performance to avoid floor and ceiling effects and could, therefore,

differ from mouse to mouse. The behavioral experiments were run using custom MATLAB (MathWorks) scripts interfacing with a National Instruments board (NI USB-6501) for reward delivery and lick registration. The stimuli were presented using Psychtoolbox through a free-field speaker (Vifa, Avisoft Bioacoustics, Germany), positioned about ~15 cm from the snout of the mouse. Stimuli were calibrated using a Pettersson M500 microphone, which was itself referenced to a sound-level calibrator (Iso-Tech SLC-1356). Stimulus levels were calibrated by integrating the recorded RMS of clicks over the mouse hearing range (1-100 kHz) and comparing this to the RMS of stimuli from the reference sound-level calibrator.

In the optogenetics experiments, the behavioral task was identical except that a single sound level (80 dB SPL) was used and on 50% of the trials bilateral photostimulation (20 Hz, 10 ms pulses, 0.2 mW/mm^2) was performed via two 470 nm LEDs (CREE-XP-E2, LED-Tech, Germany) positioned above the cranial windows. LED-on and LED-off trials were randomly interleaved and stimulation lasted for 700 ms starting 50 ms before trial onset. Furthermore, masking flashes were presented on all trials from two bright LEDs (60 mW) positioned a few cm in front of the animals' eyes.

Two-photon calcium imaging. Imaging was performed at a depth of 50 µm – 150 µm from the IC surface using a commercial two-photon laser-scanning microscope (B-Scope, ThorLabs, VA, USA), a SpectraPhysics Mai-Tai eHP laser (Spectra-Physics, CA, USA) tuned to 930 nm, and a Nikon 16x 0.8 NA objective. Images were acquired with a resolution of 512 by 512 pixels at a rate of ~28 Hz. The size of the field of view was either 500 µm by 500 µm or 666 µm by 666 µm, which allowed us to, typically, image dozens of corticorecipient IC neurons simultaneously. Each imaging session lasted around 1-2 hours.

Image processing. Rigid and non-rigid image registration, segmentation, neuropil and signal extraction were performed using the Python version of suite2p (Pachitariu et al. 2017). Neuropil extraction was performed using default suite2p parameters (https://suite2p.readthedocs.io/en/latest/settings.html), neuropil correction was done using a coefficient of 0.7 and calcium ΔF/F signals were obtained by using the median over the entire fluorescence trace as F_0. To remove slow fluctuations in the signal, a baseline of each neuron's entire trace was calculated by Gaussian filtering as well as minimum and maximum filtering using default suite2p parameters. This baseline was then subtracted from the signal. To assess the extent of image displacement in the z-axis, we compared the average of the top and the bottom 500 frames of each spatial principal component (PC) of the registered images for every 8-16 minutes of the recordings. Any region of interest (ROI) with substantial z-axis movement was excluded from further analysis. Sessions in which the majority of ROIs had to be excluded were discarded entirely. Furthermore, in order to specifically assess brain motion caused by the motor component of the task, i.e. the animal's licking, lick-triggered movies of the imaging frames were created for every 8-16 minutes of the recordings. The rationale here is that if licking causes a stereotypical displacement of the imaging plane, this will become apparent when image sequences are averaged across lick events. Specifically, non-registered image sequences surrounding (from 2 s before to 2 s after) lick events were used to produce averaged lick-triggered movies. These lick-triggered movies, as well as non-averaged sequences, were then visually inspected and ROIs were excluded from subsequent analysis if they were affected by substantial z-motion.

Analysis of task-modulated and sound-driven neurons. To identify individual neurons that produced significantly different response magnitudes in hit and miss trials, we calculated the mean activity for each stimulus trial by taking the mean activity over the 5 seconds following stimulus presentation and subtracting the mean activity over the 2 seconds preceding the stimulus during that same trial. A Mann-Whitney U test was then performed to assess whether a neuron showed a statistically significant difference (Benjamini-Hochberg adjusted p-value of 0.05) in response magnitude between hit and miss trials. The analysis was performed using equal numbers of hit and miss trials at each sound level to ensure balanced sound level distributions. If, for a given sound level, there were more hit than miss trials, we randomly selected a sample of hit trials (without substitution) to match the sample size for the miss trials and vice versa. Sound-driven neurons were identified by comparing the mean miss trial activity before and after stimulus presentation. Specifically, we performed a Mann-Whitney U test to assess whether there was a statistically significant difference (Benjamini-Hochberg adjusted p-value of 0.05) between the mean activity over the 2 seconds preceding the stimulus and the mean activity over the 1 second period following stimulus presentation. This analysis was performed using miss trials with click intensities from 53 dB SPL to 65 dB SPL (many sessions contained very few or no miss trials for higher sound levels).

Clustering analysis. To identify sub-populations of neurons with distinct response profiles, a clustering analysis was performed. While clustering is a useful approach for organizing and visualizing the activity of large and heterogeneous populations of neurons, we need to be mindful that, given continuous distributions of response properties, the locations of cluster boundaries can be somewhat arbitrary and/or reflect idiosyncrasies of the chosen method and thus vary from one algorithm to another. We employed an approach very similar to that described in Namboodiri et al. (2019) because it is thought to produce stable results in high-dimensional neural data (Hirokawa et al. 2019). For each neuron, the trial-averaged activity was obtained by averaging across all the sound levels presented in a given session separately for hit and miss trials (given the small number of catch trials, approximately one tenth of all trials, this analysis was restricted to stimulus trials only). Differences in the field of view size between sessions resulted in slight differences in frame rate and thus frame duration. Therefore, the activity traces were linearly interpolated to have the same number of data points (193 frames). For each neuron, the trial-averaged activity for miss trials was appended to that for hit trials, producing 386 data points per neuron for a total of 2649 neurons (n = 1697 neurons from 40 sessions with 9 non-lesioned mice; n = 952 neurons from 40 sessions with 7 lesioned mice). To reduce the dimensionality of this dataset before applying the clustering algorithm, we performed principal components analysis (PCA) along the time axis to capture the temporal response profile for each neuron. Guided by the 'elbow' point in a scree plot visualizing the fraction of variance explained by each PC, we decided to project the dataset to the lower dimensional subspace formed by the first 9 PCs.

Spectral clustering was used to cluster the resulting data. The affinity matrix was constructed by computing a graph of nearest neighbors. The hyperparameters of the clustering algorithm, including the number of nearest neighbors and the number of clusters, were optimized by a grid search to maximize the mean Silhouette Score for all samples. The Silhouette Score is a measure of the compactness of individual clusters (intra-cluster distance) and the separation amongst clusters (inter-cluster distance). For a given sample i that belongs to cluster C_I, the Silhouette Score is defined as:

$$s_i = \frac{(b_i - a_i)}{max(a_i, b_i)}$$

where a_i is the mean distance between sample i and all the other samples in the same cluster, and b_i is the mean distance of sample i to the nearest cluster that sample i is not part of. Let $|C_I|$ and $|C_J|$ be the number of samples belonging to clusters C_I and C_J, and $d(i,j)$ be the distance between samples i and j; a_i and b_i are defined as:

$$a_i = \frac{1}{|C_I| - 1} \sum_{j \in C_I, i \neq j} d(i,j)$$

$$b_i = \min_{J \neq I} \frac{1}{|C_J|} \sum_{j \in C_J} d(i,j)$$

The resulting clusters from the hyperparameter search were further examined by plotting clusters in pairs against each other with t-distributed Stochastic Neighbor Embedding, a statistical method for visualizing high-dimensional data that involves giving each data point a location in a two or three-dimensional space (van der Maaten and Hinton 2008).

Population decoding. Logistic regression models were trained on the network activity of each session, i.e., the ΔF/F values of all ROIs in each session, to classify hit vs miss trials. This was done on a frame-by-frame basis, meaning that each time point (frame) of each session was trained separately. Rather than including all the trials in a given session, only trials of intermediate difficulty were used for the decoding analysis. More specifically, we only included trials across five sound levels, comprising the lowest sound level that exceeded a d' of 1.5 plus the two sound levels below and above that level. That ensured that differences in sound level distributions would be small, while still giving us a sufficient number of trials to perform the decoding analysis. Sessions were only included if there were at least 15 instances for both hit and miss trials. The models were trained with L2 regularization, which gave similar contributions to correlated features (i.e., individual neuronal activity) instead of discarding some of the correlated features that were also related to behaviorally-relevant information. The strength of the regularization for each model was hyperparameter-tuned and the reported results were cross validated. Specifically, neuronal data in each session was split into 5 stratified folds, and each fold preserved the percentage of hit and miss trials in a given session. Four folds were used for cross-validated hyperparameter search (randomized search drawn from the log-uniform distribution between 1×10^{-4} and 1×10^{2}), and the remaining 1 fold was used for evaluating the model after the best hyperparameters were refitted on the 4 folds of data. To more reliably estimate the model results, the evaluation was done for each of the 5 folds for each session and the average of these 5 results was taken as each session's model performance at each timepoint.

The percentage of hit and miss trials was different in each session, and the number of hit trials often exceeded the number of miss trials. To include as many trials as possible while preventing the models from taking advantage of class imbalances, balancing procedures were performed at both the model-level and the metrics-level. First, logistic regression was trained

with the class weights adjusted inversely proportional to the frequency of each trial type in the training data, giving higher weights to the minority class and lower weights to the majority class. Given the total number of trials in the training data N_T, the number of classes N_C, and the number of trials for a given class N_i, the weight for a given class W_i was defined as follows:

$$W_i = W_T \,/\, (N_C * N_i\,)$$

These weights were then applied to the cost function during the training process to increase the penalty for minority class misclassifications and reduce the penalty for majority class misclassifications. Second, to avoid the estimated model performance being inflated due to class imbalance, balanced accuracy (Brodersen et al. 2010) was used to report the model performance. Balanced accuracy was defined as the arithmetic mean of the true positive rate and the true negative rate. For a model performing equally well on either class, the balanced accuracy is the same as the conventional accuracy (i.e., the number of correct predictions divided by the total number of predictions). However, for a model scoring above chance only because the model takes advantage of the class imbalance (i.e. consistently predicts the majority class), the balanced accuracy is at chance level.

$$Balanced\ accuracy\ = \frac{1}{2} * \left(\frac{N_{true\ pos.}}{N_{true\ pos.}+N_{true\ neg.}} + \frac{N_{true\ neg.}}{N_{true\ neg.}+N_{true\ pos.}}\right)$$

Additionally, dummy models were used as baseline models to compare against the performance of the logistic regression models. Dummy models predicted the class labels (i.e., hit or miss trials) randomly while taking into account the probability of each class.

To assess whether the model performance was correlated with the number of ROIs recorded in a session, Spearman's correlation coefficient was computed between the number of ROIs in a session and the mean model performance over different 1-second time periods relative to stimulus onset (from 2 seconds before to 5 seconds after stimulus onset).

Statistical tests were conducted to compare the model performance between lesioned and non-lesioned mice, as well as between the trained models and dummy models. Since the frame rate varied slightly with the size of the field of view, the numbers of frames (193 - 197 frames) per 7-s trial could be different across sessions. Thus, model performance was linearly interpolated to make all sessions contain the same number of frames before statistical tests were performed at each timepoint. The model performance of each session was cross-validated and averaged across folds, and the statistical tests were performed on the distributions of the sessions' model performance. The Shapiro–Wilk test was used to determine whether a parametric or nonparametric test should be used, using $p < 0.05$ as a criterion. A one-sided Wilcoxon signed-rank test or paired t-test was performed for comparing trained vs dummy models, while a one-sided Mann-Whitney U test or t-test was performed for comparing trained models for different groups of mice. Because of the smaller sample sizes, the statistical tests in Figure 6B were carried out after binning the scores for every two timepoints. Statistical significance was defined as $p < 0.05$ after Bonferroni correction.

Data availability. Data will be made available in a public repository.

Acknowledgments. We are grateful to Christopher Breen and Robert Campbell for helping with the histology, to Ben Willmore for help with implementing the decoding analysis and for

772 the financial assistance provided by an Oxford-Taiwan Graduate Scholarship from the
773 University of Oxford and the Taiwan Ministry of Education to TYL, a Wellcome 4 year PhD
774 Studentship to YW (102372/Z/13/Z), and by a Wellcome Principal Research Fellowship to AJK
775 (WT108369/Z/2015/Z). This research was funded in whole, or in part, by the Wellcome Trust
776 [102372/Z/13/Z; WT108369/Z/2015/Z]. For the purpose of Open Access, the author has
777 applied a CC BY public copyright licence to any Author Accepted Manuscript version arising
778 from this submission.

779

780 **References**

781 Antunes FM, Malmierca MS. 2021. Corticothalamic Pathways in Auditory Processing: Recent
782 Advances and Insights From Other Sensory Systems. Frontiers in Neural Circuits.
783 doi:10.3389/fncir.2021.721186

784 Bajo VM, King AJ. 2013. Cortical modulation of auditory processing in the midbrain. Frontiers
785 in Neural Circuits **6**:114. doi:10.3389/fncir.2012.00114

786 Barnstedt O, Keating P, Weissenberger Y, King AJ, Dahmen JC. 2015. Functional
787 Microarchitecture of the Mouse Dorsal Inferior Colliculus Revealed through In Vivo Two-
788 Photon Calcium Imaging. Journal of Neuroscience **35**:10927–10939.
789 doi:10.1523/JNEUROSCI.0103-15.2015

790 Blackwell JM, Lesicko AM, Rao W, De Biasi M, Geffen MN. 2020. Auditory cortex shapes
791 sound responses in the inferior colliculus. eLife. doi:10.7554/elife.51890

792 Brodersen KH, Ong CS, Stephan KE, Buhmann JM. 2010. The Balanced Accuracy and Its
793 Posterior Distribution. doi:10.1109/icpr.2010.764

794 Buser PA, Imbert M. 1992. Audition. Cambridge, Mass.: MIT Press.

795 Casseday JH, Covey E. 1996. A neuroethological theory of the operation of the inferior
796 colliculus. Brain, behavior and evolution **47**:311–336. doi:10.1159/000113249

797 Ceballo S, Piwkowska Z, Bourg J, Daret A, Bathellier B. 2019. Targeted Cortical Manipulation
798 of Auditory Perception. Neuron **104**:1168-1179.e5. doi:10.1016/j.neuron.2019.09.043

799 Chen C, Song S. 2019. Differential cell-type dependent brain state modulations of sensory
800 representations in the non-lemniscal mouse inferior colliculus. Communications Biology **2**:356.
801 doi:10.1038/s42003-019-0602-4

802 Chen CC, Cheng MM, Ito T, Song SS. 2018. Neuronal Organization in the Inferior Colliculus
803 Revisited with Cell-Type-Dependent Monosynaptic Tracing. The Journal of Neuroscience.
804 doi:10.1523/jneurosci.2173-17.2018

805 Coleman JR, Clerici WJ. 1987. Sources of projections to subdivisions of the inferior colliculus
806 in the rat. Journal of comparative neurology (1911) **262**:215–226. doi:10.1002/cne.902620204

807 Cruces-Solís H, Jing Z, Babaev O, Rubin J, Gür B, Krueger-Burg D, Strenzke N, De Hoz L.
808 2018a. Auditory midbrain coding of statistical learning that results from discontinuous sensory
809 stimulation. PLOS Biology. doi:10.1371/journal.pbio.2005114

810 De Franceschi G, Barkat TR. 2021. Task-induced modulations of neuronal activity along the
811 auditory pathway. Cell reports (Cambridge) **37**:110115. doi:10.1016/j.celrep.2021.110115

812 Engel AK, Fries P, Singer W. 2001. Dynamic predictions: oscillations and synchrony in top-
813 down processing. Nature reviews. Neuroscience **2**:704–716. doi:10.1038/35094565

814 Francis NA, Winkowski DE, Sheikhattar A, Armengol K, Babadi B, Kanold PO. 2018. Small
815 Networks Encode Decision-Making in Primary Auditory Cortex. Neuron (Cambridge, Mass.)
816 **97**:885-897.e6. doi:10.1016/j.neuron.2018.01.019

817 Gimenez TL, Lorenc M, Jaramillo S. 2015. Adaptive categorization of sound frequency does
818 not require the auditory cortex in rats. Journal of Neurophysiology 114:1137-1145. Doi:
819 10.1152/jn.00124.2015

820 Hirokawa J, Vaughan A, Masset P, Ott T, Kepecs A. 2019. Frontal cortex neuron types
821 categorically encode single decision variables. Nature 576, 446-451. Doi: 10.1038/s41586-
822 019-1816-9

Hong YK, Lacefield CO, Rodgers CC, Bruno RM. 2018. Sensation, movement and learning in the absence of barrel cortex. Nature **561**:542–546. doi:10.1038/s41586-018-0527-y

Huffman RF, Henson OW. 1990. The descending auditory pathway and acousticomotor systems: connections with the inferior colliculus. Brain Research Reviews **15**:295–323. doi:10.1016/0165-0173(90)90005-9

Inagaki HK, Chen S, Ridder MC, Sah P, Li N, Yang Z, Hasanbegovic H, Gao Z, Gerfen CR, Svoboda K. 2022. A midbrain-thalamus-cortex circuit reorganizes cortical dynamics to initiate movement. Cell 185, 1065-1081. doi: 10.1016/j.cell.2022.02.006

Kato HK, Gillet SN, Isaacson JS. 2015. Flexible Sensory Representations in Auditory Cortex Driven by Behavioral Relevance. Neuron **88**:1027–1039. doi:10.1016/j.neuron.2015.10.024

Keck T, Keller GB, Jacobsen RI, Eysel UT, Bonhoeffer T, Hübener M. 2013. Synaptic Scaling and Homeostatic Plasticity in the Mouse Visual Cortex In Vivo. NEURON **80**:327–334. doi:10.1016/j.neuron.2013.08.018

Kelly, Buzzard Jack. 1970. The effects of lateral lemniscal and neocortical lesions on auditory absolute thresholds and frequency difference thresholds of the rat . Vanderbilt.

King AJ, Bajo VM, Nodal FR, Moore DR. 2010. The descending corticocollicular pathway mediates learning-induced auditory plasticity. Nature neuroscience **13**:253–260. doi:10.1038/nn.2466

Kraus N, White-Schwoch T. 2015. Unraveling the Biology of Auditory Learning: A Cognitive–Sensorimotor–Reward Framework. Trends in cognitive sciences **19**:642–654. doi:10.1016/j.tics.2015.08.017

Lee S-H, Dan Y. 2012. Neuromodulation of Brain States. Neuron **76**:209–222. doi:10.1016/j.neuron.2012.09.012

Lesicko AMH, Hristova TS, Maigler KC, Llano DA. 2016. Connectional Modularity of Top-Down and Bottom-Up Multimodal Inputs to the Lateral Cortex of the Mouse Inferior Colliculus. The Journal of Neuroscience. doi:10.1523/jneurosci.4134-15.2016

Li J, Liao X, Zhang Jianxiong, Wang M, Yang N, Zhang Jun, Lv G, Li H, Lu J, Ding R, Li X, Guang Y, Yang Z, Qin H, Jin W, Zhang K, He C, Jia H, Zeng S, Hu Z, Nelken I, Chen X. 2017. Primary Auditory Cortex is Required for Anticipatory Motor Response. Cerebral Cortex. doi:10.1093/cercor/bhx079

Liu M, Xie F, Dai J, Zhang J, Yuan K, Wang N. 2023. Brain-wide inputs to the non-lemniscal inferior colliculus in mice. Neuroscience letters **793**:136976. doi:10.1016/j.neulet.2022.136976

Lohse M, Bajo VM, King AJ, Willmore BDB. 2020. Neural circuits underlying auditory contrast gain control and their perceptual implications. Nature Communications **11**:324. doi:10.1038/s41467-019-14163-5

Malmierca MS, Anderson LA, Antunes FM. 2015. The cortical modulation of stimulus-specific adaptation in the auditory midbrain and thalamus: a potential neuronal correlate for predictive coding. Frontiers in systems neuroscience **9**:19. doi:10.3389/fnsys.2015.00019

Mccormick DA, Nestvogel DB, He BJ. n.d. Neuromodulation of Brain State and Behavior. doi:10.1146/annurev-neuro-100219-

McGinley MJ, Vinck M, Reimer J, Batista-Brito R, Zagha E, Cadwell CR, Tolias AS, Cardin JA, McCormick DA. 2015. Waking State: Rapid Variations Modulate Neural and Behavioral Responses. Neuron **87**:1143–1161. doi:10.1016/j.neuron.2015.09.012

Mettler FA. 1935. Corticifugal fiber connections of the cortex of Macaca mulatta. The temporal region. Journal of comparative neurology (1911) **63**:25–47. doi:10.1002/cne.900630104

868 Metzger RR, Greene NT, Porter KK, Groh JM. 2006. Effects of Reward and Behavioral
869 Context on Neural Activity in the Primate Inferior Colliculus. The Journal of neuroscience
870 **26**:7468–7476. doi:10.1523/JNEUROSCI.5401-05.2006

871 Moriizumi T, Hattori T. 1991. Pallidotectal projection to the inferior colliculus of the rat.
872 Experimental brain research **87**:223–226. doi:10.1007/BF00228524

873 Musall S, Kaufman MT, Juavinett AL, Gluf S, Churchland AK. 2019. Single-trial neural
874 dynamics are dominated by richly varied movements. Nature Neuroscience.
875 doi:10.1038/s41593-019-0502-4

876 Nakamoto KT, Jones SJ, Palmer AR. 2008. Descending Projections From Auditory Cortex
877 Modulate Sensitivity in the Midbrain to Cues for Spatial Position. Journal of Neurophysiology
878 **99**:2347–2356. doi:10.1152/jn.01326.2007

879 Namboodiri VMK, Otis JM, Van Heeswijk K, Voets ES, Alghorazi RA, Rodriguez-Romaguera
880 J, Mihalas S, Stuber GD. 2019. Single-cell activity tracking reveals that orbitofrontal neurons
881 acquire and maintain a long-term memory to guide behavioral adaptation. Nature
882 Neuroscience. doi:10.1038/s41593-019-0408-1

883 Nienhuis R, Olds J. 1978. Changes in unit responses to tones after food reinforcement in the
884 auditory pathway of the rat: Intertrial arousal. Experimental Neurology. doi:10.1016/0014-
885 4886(78)90152-8

886 Noudoost B, Chang MH, Steinmetz NA, Moore T. 2010. Top-down control of visual attention.
887 Current opinion in neurobiology **20**:183–190. doi:10.1016/j.conb.2010.02.003

888 Oberle HM, Ford AN, Dileepkumar D, Czarny J, Apostolides PF. 2022a. Synaptic mechanisms
889 of top-down control in the non-lemniscal inferior colliculus. eLife. doi:10.7554/elife.72730

Olaźbal UE, Moore JK. 1989. Nigrotectal projection to the inferior colliculus: Horseradish peroxidase transport and tyrosine hydroxylase immunohistochemical studies in rats, cats, and bats. Journal of comparative neurology (1911) **282**:98–118. doi:10.1002/cne.902820108

O'sullivan C, Weible AP, Wehr M. 2019. Auditory Cortex Contributes to Discrimination of Pure Tones. eneuro. doi:10.1523/eneuro.0340-19.2019

Otchy TM, Wolff SBE, Rhee JY, Pehlevan C, Kawai R, Kempf A, Gobes SMH, Ölveczky BP. 2015. Acute off-target effects of neural circuit manipulations. Nature. doi:10.1038/nature16442

Pachitariu M, Stringer C, Dipoppa M, der SS, Rossi L, Dalgleish H, Carandini M, Harris K. 2017. Suite2p: beyond 10,000 neurons with standard two-photon microscopy, bioRxiv. Cold Spring Harbor: Cold Spring Harbor Laboratory Press. doi:10.1101/061507

Parker PRL, Brown MA, Smear MC, Niell CM. 2020. Movement-Related Signals in Sensory Areas: Roles in Natural Behavior. Trends in neurosciences (Regular ed.) **43**:581–595. doi:10.1016/j.tins.2020.05.005

Parras GG, Nieto-Diego J, Carbajal GV, Valdés-Baizabal C, Escera C, Malmierca MS. 2017. Neurons along the auditory pathway exhibit a hierarchical organization of prediction error. Nature Communications. doi:10.1038/s41467-017-02038-6

Paxinos G, Franklin KBJ, Franklin KBJ. 2001. The mouse brain in stereotaxic coordinates. San Diego: Academic Press.

Pickles JO. 1988. An introduction to the physiology of hearing. London ; San Diego: Academic Press.

Quass GL, Rogalla MM, Ford AN, Apostolides PF. 2023. Mixed representations of sound and action in the auditory midbrain. bioRxiv. doi: 10.1101/2023.09.19.558449

912 Ruth RE, Peter Rosenfeld J, Harris DM, Birkel P. 1974. Effects of aversive and rewarding
913 electrical brain stimulation on auditory evoked responses in albino rat tectum. Physiology
914 & Behavior. doi:10.1016/0031-9384(74)90254-6

915 Saderi D, Schwartz ZP, Heller CR, Pennington JR, David SV. 2021. Dissociation of task
916 engagement and arousal effects in auditory cortex and midbrain. eLife.
917 doi:10.7554/elife.60153

918 Shaheen LA, Slee, SJ, David, SV. 2021. Task engagement improves neural discriminability in
919 the auditory midbrain of the marmoset monkey. Journal of Neuroscience. 41(1):284-297. doi:
920 10.1523/JNEUROSCI.1112-20.2020

921 Schneider DM, Mooney R. n.d. Annual Review of Neuroscience How Movement Modulates
922 Hearing. doi:10.1146/annurev-neuro-072116-

923 Schneider DM, Nelson A, Mooney R. 2014. A synaptic and circuit basis for corollary discharge
924 in the auditory cortex. Nature **513**:189–194. doi:10.1038/nature13724

925 Sherman SM. 2007. The thalamus is more than just a relay. Current opinion in neurobiology
926 **17**:417–422. doi:10.1016/j.conb.2007.07.003

927 Shore SE, Zhou J. 2006. Somatosensory influence on the cochlear nucleus and beyond.
928 Hearing research **216**:90–99. doi:10.1016/j.heares.2006.01.006

929 Singla S, Dempsey C, Warren R, Enikolopov AG, Sawtell NB. 2017. A cerebellum-like circuit
930 in the auditory system cancels responses to self-generated sounds. Nature neuroscience
931 **20**:943–950. doi:10.1038/nn.4567

932 Song Y-H, Kim J-H, Jeong H-W, Choi I, Jeong D, Kim K, Lee S-H. 2017. A Neural Circuit for
933 Auditory Dominance over Visual Perception. Neuron (Cambridge, Mass.) **93**:940-954.e6.
934 doi:10.1016/j.neuron.2017.01.006

Stebbings KA, Lesicko AMH, Llano DA. 2014. The auditory corticocollicular system: Molecular and circuit-level considerations. Hearing research **314**:51–59. doi:10.1016/j.heares.2014.05.004

Stringer C, Pachitariu M, Steinmetz N, Reddy CB, Carandini M, Harris KD. 2019. Spontaneous behaviors drive multidimensional, brainwide activity. Science. doi:10.1126/science.aav7893

Suga N. 2008. Role of corticofugal feedback in hearing. Journal of Comparative Physiology **194**:169–183. doi:10.1007/s00359-007-0274-2

Talwar SK, Musial PG, Gerstein GL. 2001. Role of Mammalian Auditory Cortex in the Perception of Elementary Sound Properties. Journal of Neurophysiology **85**:2350–2358. doi:10.1152/jn.2001.85.6.2350

van der Maaten L, Hinton G. 2008. Visualizing Data using t-SNE Laurens van der Maaten. Journal of Machine Learning Research.

Vila C-H, Williamson RS, Hancock KE, Polley DB. 2019. Optimizing optogenetic stimulation protocols in auditory corticofugal neurons based on closed-loop spike feedback. Journal of Neural Engineering. doi:10.1088/1741-2552/ab39cf

Wenstrup JJ, Larue DT, Winer JA. 1994. Projections of physiologically defined subdivisions of the inferior colliculus in the mustacbed bat: Targets in the medial geniculate body and extrathalamic nuclei. Journal of comparative neurology (1911) **346**:207–236. doi:10.1002/cne.903460204

Wiegert JS, Mahn M, Prigge M, Printz Y, Yizhar O. 2017. Silencing Neurons: Tools, Applications, and Experimental Constraints. Neuron **95**:504–529. doi:10.1016/j.neuron.2017.06.050

Winer JA. 2005. Decoding the auditory corticofugal systems. Hearing research **207**:1–9. doi:10.1016/j.heares.2005.06.007

959 Xiong XR, Liang F, Zingg B, Ji X, Ibrahim LA, Tao HW, Zhang LI. 2015. Auditory cortex
960 controls sound-driven innate defense behaviour through corticofugal projections to inferior
961 colliculus. Nature Communications **6**:7224. doi:10.1038/ncomms8224

962 Yang Y, Lee J, Kim G. 2020. Integration of locomotion and auditory signals in the mouse
963 inferior colliculus. eLife. doi:10.7554/elife.52228

964 Zingg B, Chou X, Zhang Z, Mesik L, Liang F, Tao HW, Zhang LI. 2017. AAV-Mediated
965 Anterograde Transsynaptic Tagging: Mapping Corticocollicular Input-Defined Neural
966 Pathways for Defense Behaviors. Neuron (Cambridge, Mass.) **93**:33–47.
967 doi:10.1016/j.neuron.2016.11.045

968
969
970
971
972
973
974
975
976
977
978
979
980
981
982
983
984
985
986
987

Figure supplements

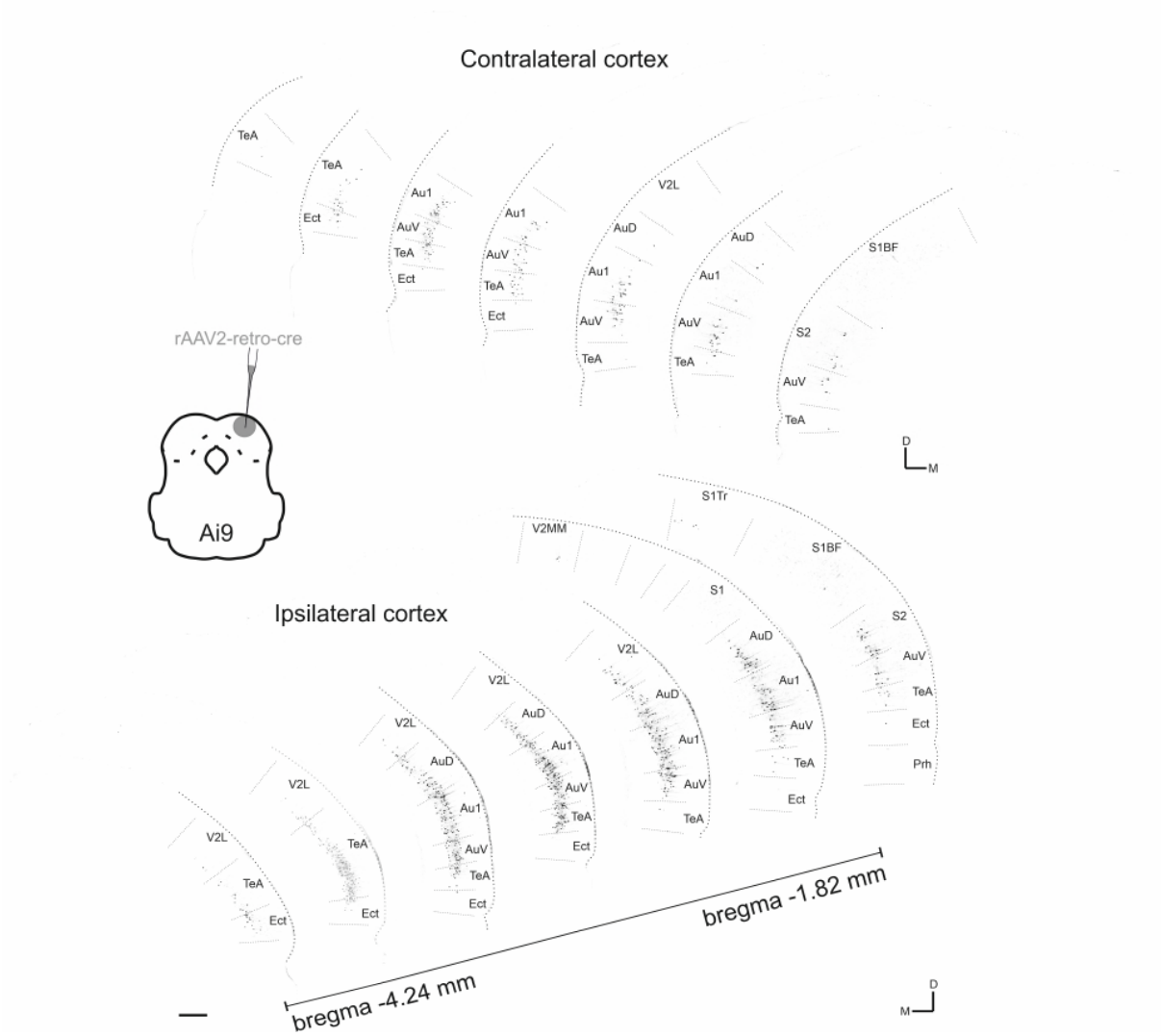

Figure 2 - figure supplement 1. Contra- and ipsilateral corticocollicular neurons along the rostrocaudal axis. Seven coronal sections are shown from each hemisphere covering approximately 2.5 mm of the rostrocaudal axis. Corticocollicular neurons were labeled by injecting a total of 150 nL of rAAV2-CAG-cre into the dorsal IC (at three sites and several depths from 100 µm - 400 µm below the brain surface) of a tdTomato reporter mouse (Ai9). Data were obtained using whole-brain laser scanning two-photon tomography. The resulting images were grayscale inverted and thresholded to remove all background labeling so that they could be more easily arranged into a common figure. Area borders were drawn onto the images according to Paxinos and Franklin (2001). Cortical area abbreviations: Au1, primary auditory; AuD, secondary auditory, dorsal; AuV, secondary auditory, ventral; Ect, ectorhinal; Prh, perirhinal; S1, primary somatosensory; S1BF, primary somatosensory, barrel field; S1Tr, primary somatosensory, trunk region; S2, secondary somatosensory; TeA, temporal association; V2L, secondary visual, lateral. Scale bar, 200 µm.

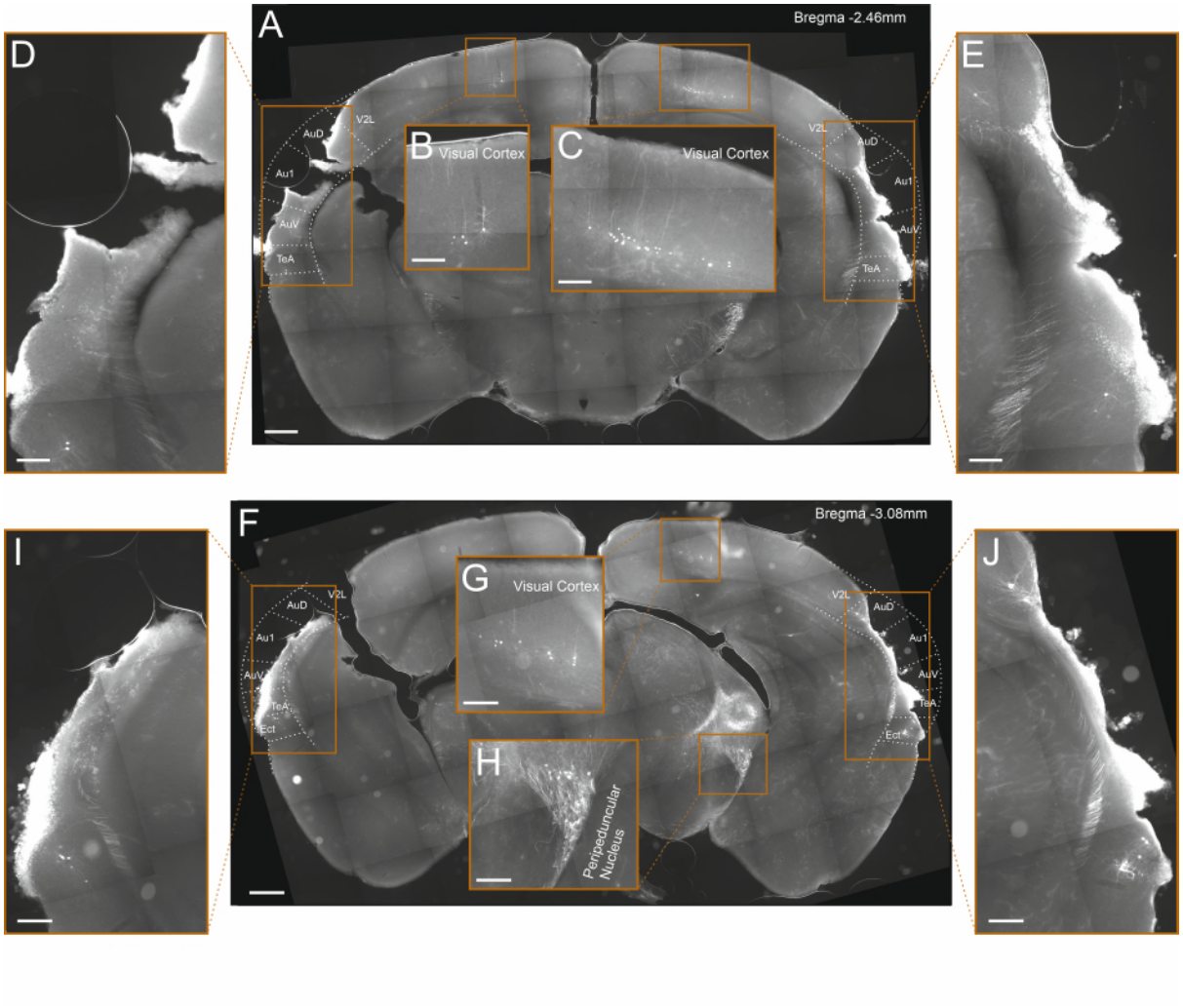

Figure 2 - figure supplement 2. Lesioning by thermocoagulation. (**A**) Coronal section showing lesion extent in a mouse that had undergone lesioning by thermocoagulation. After data collection had been completed, rAAV2-retro-tdTomato was injected along the dorsal IC in order to label corticocollicular neurons that had remained intact. Area borders were drawn onto the images according to Paxinos and Franklin (2001). Scale bar, 500 µm. (**B**,**C**) Higher magnification images showing tdTomato-labeled corticocollicular neurons in the left and right visual cortex. Scale bars, 200 µm. (**D**,**E)** Higher magnification images of the temporal regions surrounding the lesion sites, showing a very small number of residual corticocollicular neurons in the left and right temporal association area and the right dorsal auditory field. Scale bars, 200 µm. (**F)** Same as **A** for a different coronal section of the same mouse. (**G**,**H**) Higher magnification images showing tdTomato-labeled corticocollicular neurons in the right visual cortex and thalamocollicular neurons in the right peripeduncular nucleus. Scale bars, 200 µm. (**I**,**J)** Higher magnification images of the temporal regions surrounding the lesion sites showing a very small number of residual corticocollicular neurons in the left and right ectorhinal cortex and the right dorsal auditory field. Scale bars, 200 µm. While the lesion procedure spared some auditory cortex tissue in this animal, its visual appearance and the fact that barely any corticocollicular neurons could be found suggests that this residual tissue was almost completely destroyed. Consequently, we categorized this animal as having a (near-)complete lesion, meaning that 5% or less of the auditory cortex was left intact. Cortical area abbreviations: Au1, primary auditory; AuD, secondary auditory, dorsal; AuV, secondary auditory, ventral; Ect, ectorhinal; TeA, temporal association; V2L, secondary visual, lateral;

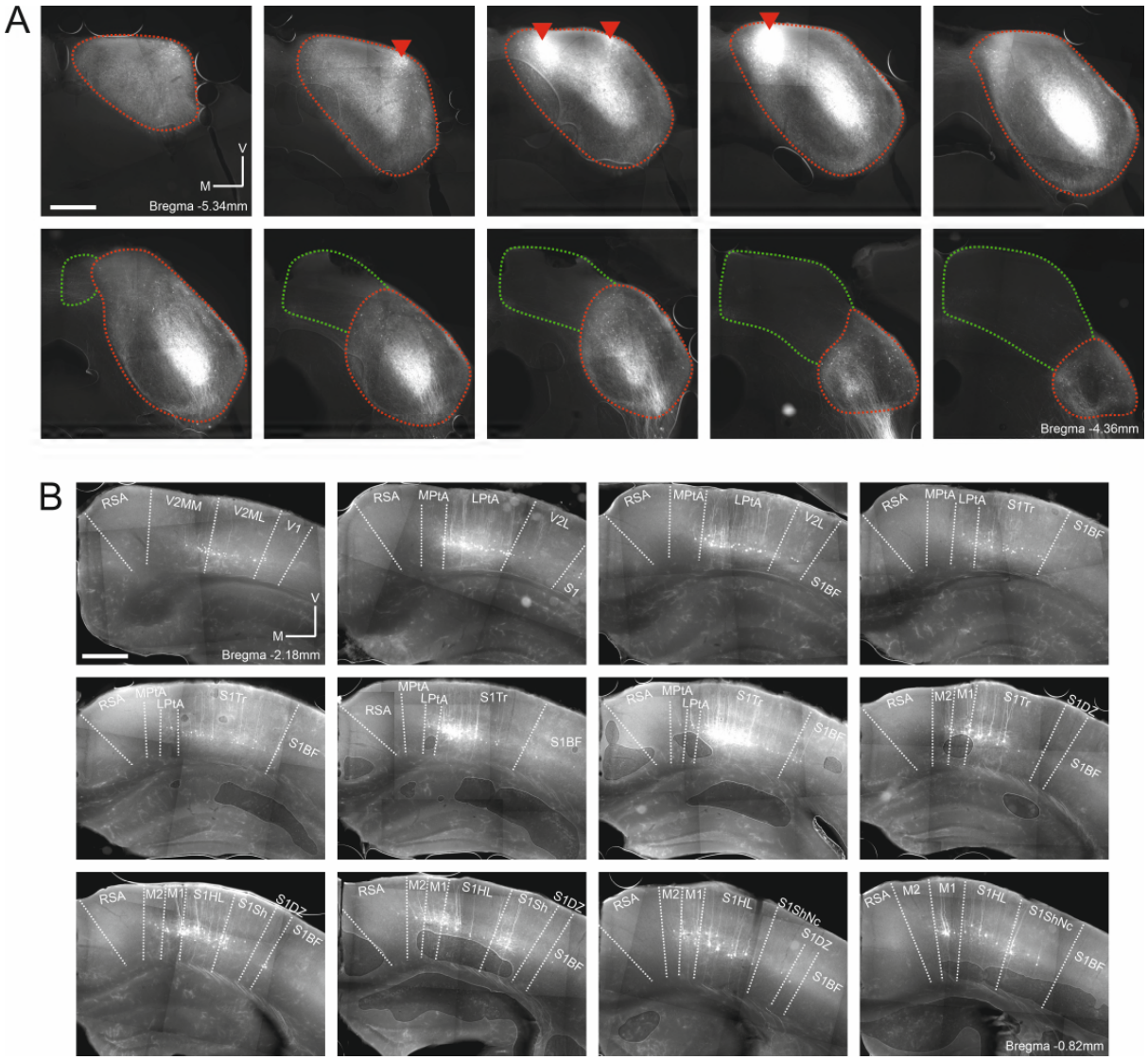

Figure 2 - figure supplement 3. Retrograde labeling of corticocollicular neurons in non-temporal areas of the cerebral cortex is not the result of viral leakage into the superior colliculus. (**A**) Coronal sections showing the right midbrain of one example mouse (same mouse as in Figure 2 - figure supplement 2). Sections are ordered caudo-rostrally from top left to bottom right. Red lines indicate the approximate outline of the inferior colliculus, green lines the approximate outline of the superior colliculus. Red triangles indicate rAAV2-retro-tdTomato injection locations. In addition to the labeling near the injection sites, widespread retrograde labeling is found in the central nucleus of the inferior colliculus. No labeled cell bodies were found in the superior colliculus. Scale bar, 500 µm. (**B**) Coronal sections showing corticocollicular neurons in non-temporal areas of the right cerebral cortex labeled as a result of the rAAV2-retro-tdTomato injections in the inferior colliculus illustrated in **A**. Sections are ordered caudo-rostrally from top left to bottom right. Area borders were drawn onto the images according to Paxinos and Franklin (2001). Scale bar, 500 µm. Cortical area abbreviations: LPta, lateral parietal association; MPta, medial parietal association; M1: primary motor; M2: secondary motor; RSA, retrosplenial agranular; S1BF, primary somatosensory, barrel field; S1DZ, primary somatosensory, dysgranular region; S1HL, primary somatosensory, hindlimb region; S1Sh, primary somatosensory, shoulder region; S1ShNc, primary somatosensory, shoulder/neck region; S1Tr, primary somatosensory, trunk field; V1, primary visual; V2L, secondary visual, lateral; V2ML, secondary visual mediolateral; V2MM, secondary visual mediomedial.

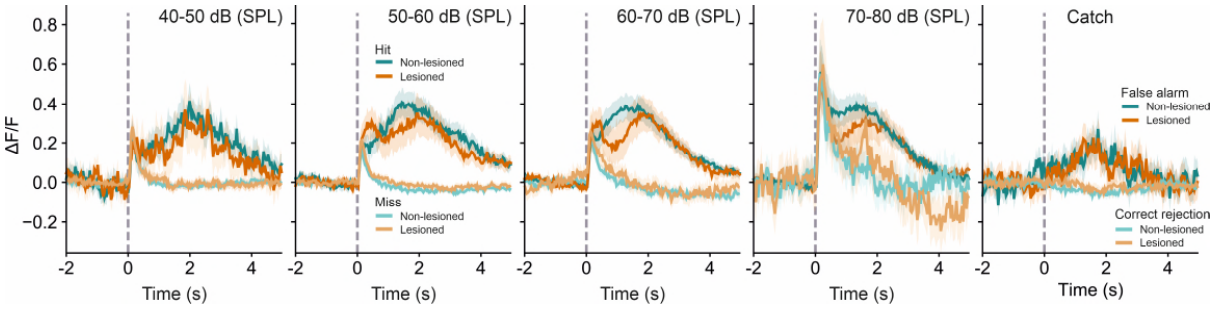

Figure 4 – figure supplement 1. Averaged response profiles for stimulus and catch trials. Stimulus trials are binned into four different sound level ranges and separated into hit and miss trials. Catch trials are separated into false alarms and correct rejections. Shaded areas represent 95% confidence intervals.

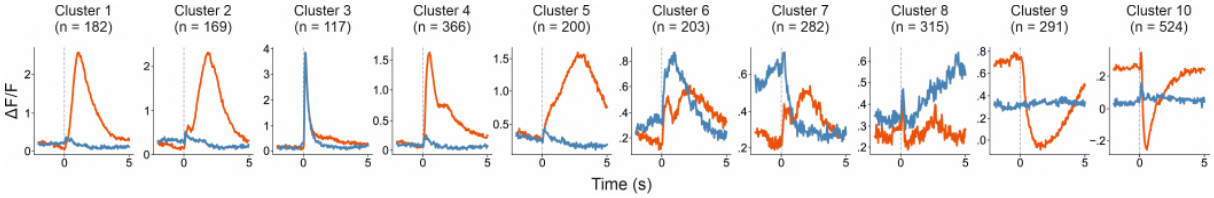

Figure 5 - figure supplement 1. Rescaled response profiles for each cluster. Averaged response profiles obtained by taking the mean across all neurons in a cluster separately for hit (red) and miss (blue) trials. Same as Figure 5B except that here each panel has an individualized y-axis range.

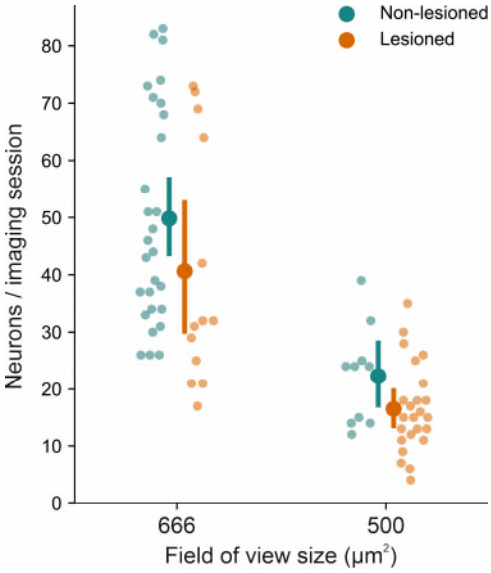

Figure 5 - figure supplement 2. Number of sessions for each imaging field of view size. A greater number of recordings happened to be made with the larger field of view in non-lesioned (28 of 38) than in lesioned (13 of 37) mice. Consequently, the number of neurons recorded in non-lesioned mice was greater than that recorded in lesioned mice (1697 vs 952). Error bars represent 95% confidence intervals.

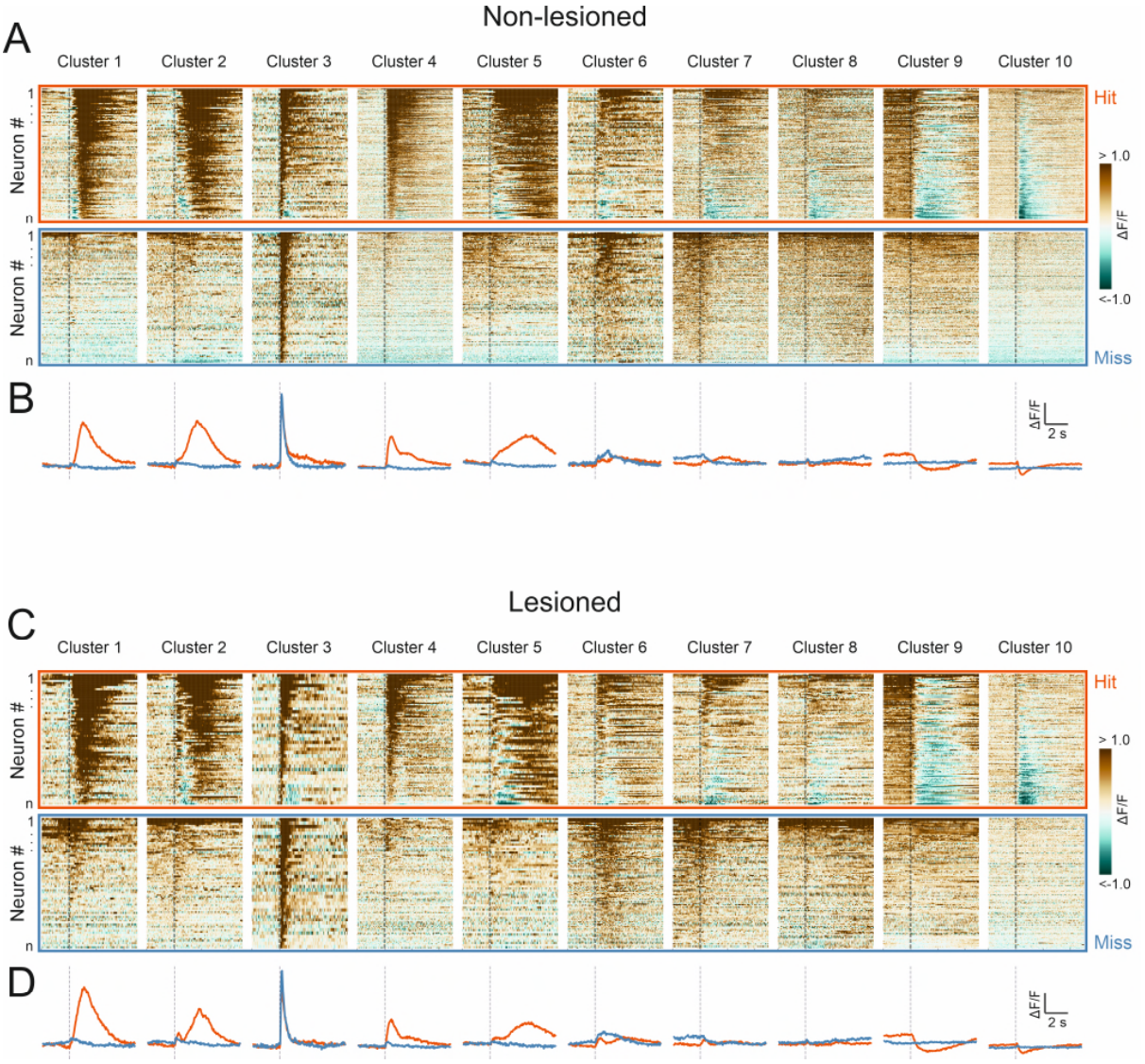

Figure 5 – figure supplement 3. High correspondence between cluster profiles of lesioned and non-lesioned mice. (**A**) Peri-stimulus time histograms for all neurons recorded in non-lesioned mice separated by cluster identity: hit trials (top) vs miss trials (bottom). (**B**) Averaged response profiles obtained by taking the mean across all neurons in each cluster separately for hit (red) and miss (blue) trials. (**C, D**) Same as **A** and **B** for neurons recorded in lesioned mice.

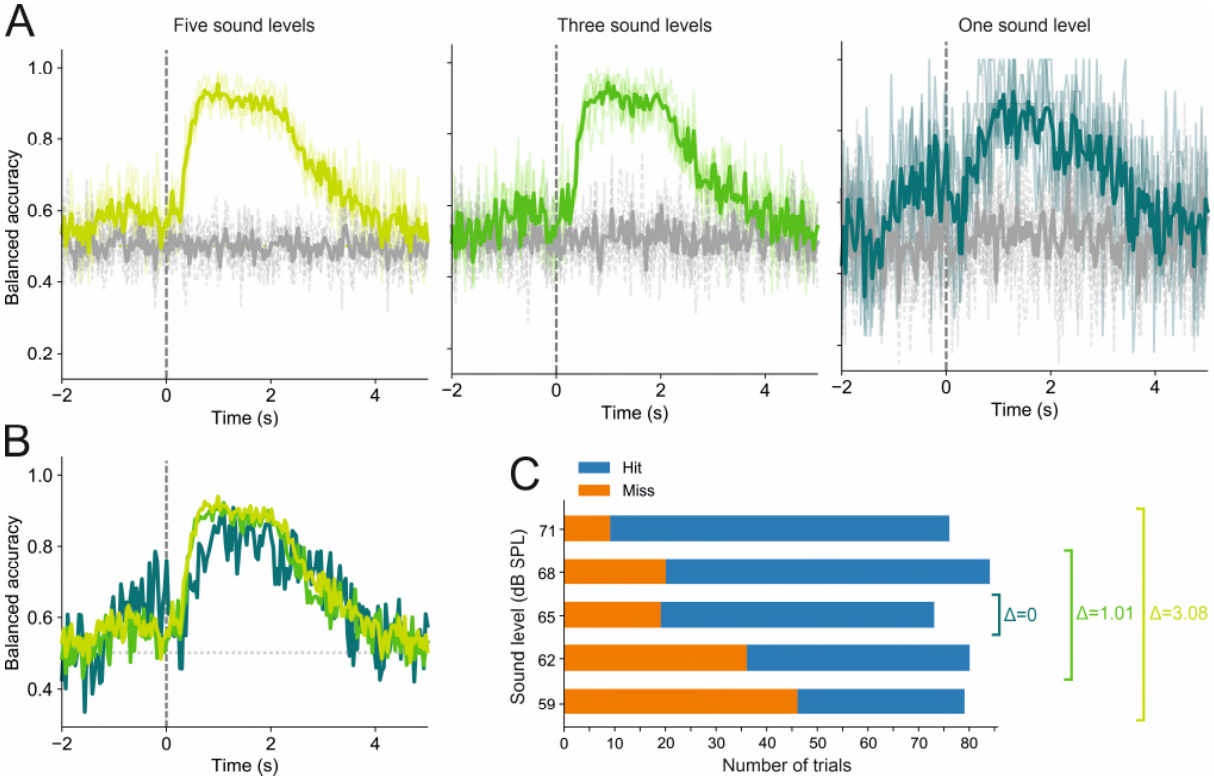

Figure 6 – figure supplement 1. Trial outcome decoding is not meaningfully affected by differences in sound level distributions between hit and miss trials. (**A**) Decoding results for one imaging session based on trials in which stimuli were presented at five (left), three (middle), or a single sound level (right). Thin colored lines show the results of each of the five cross-validation folds. Thick colored lines indicate averages across all five folds. Gray lines show results for the corresponding dummy models. (**B**) Superimposed averages from **A**. (**C**) Hit and miss trial distributions for each of the five sound levels, as well as the mean sound level difference (Δ) between hit and miss trials for the three decoding conditions shown in **A** and **B**. The mean difference was 3.08 dB, 1.01 dB and 0 dB for the five, three and one sound level condition, respectively.

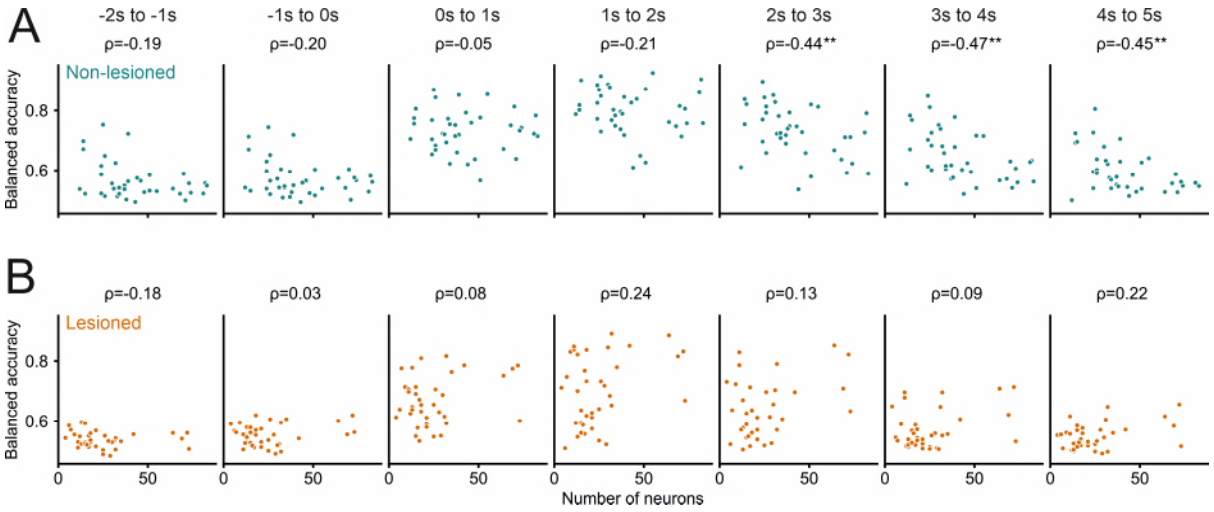

Figure 6 - figure supplement 2. Greater number of recorded neurons was not associated with better decoding performance. **(A,B)** Decoding performance (balanced accuracy) of the logistic regression models averaged over different 1-s time periods relative to stimulus onset as a function of the number of neurons recorded in a given session. A greater number of neurons obtained in a field of view was not associated with better decoding performance. Values above panels indicate Spearman's rank correlation coefficient ρ. The only statistically significant relationship between the number of recorded neurons and decoding performance was found for late trial periods in non-lesioned mice (A), and indicated that for time periods >2 seconds after stimulus onset a smaller sample size was associated with better decoding performance. **: $p < 0.01$.

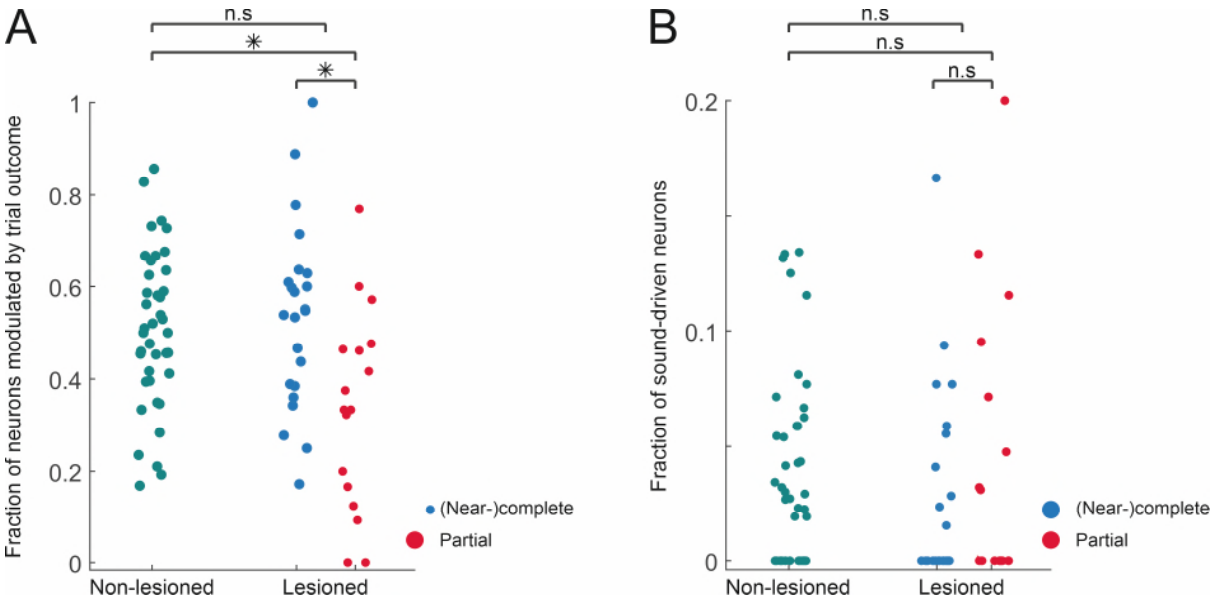

Figure 6 - figure supplement 3. Similar fractions of task-modulated and sound-driven neurons in lesioned and non-lesioned mice. (**A**) Fraction of neurons per session that exhibit a significant difference in response magnitude between hit and miss trials. (**B**) Fraction of neurons per session that exhibit a significant stimulus response in miss trials. *: $p < 0.01$, Mann Whitney U test.

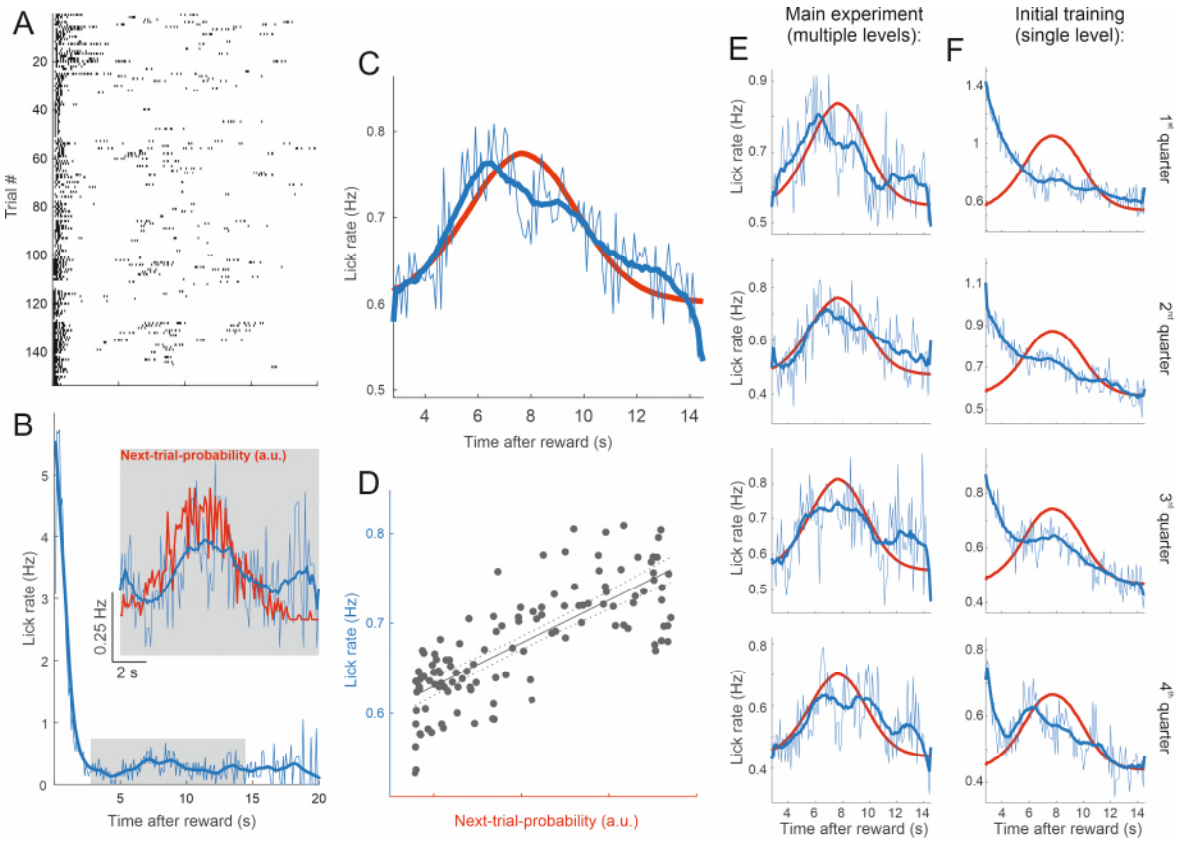

Figure 6 - figure supplement 4. Lick rates in peri-catch trial periods approximate next-trial-probability. (**A**) Peri-catch trial lick raster for all catch trials that followed a hit trial for one example mouse. The peri-catch trial period was defined as the period from the reward delivery in the hit trial to the onset of the trial following the catch trial. (**B**) Lick rate averaged across the peri-catch trial periods shown in **A** and binned into 100ms wide bins. The thick blue line shows the smoothed (20-point running average) lick rate. The inset gives a magnified view of the average lick rate during the period indicated by the gray rectangle. The red line illustrates the distribution of 'reward-to-next-trial-onset' intervals experienced by the example mouse. Given that licks are plotted time-locked to reward delivery, we plotted the distribution of intervals between reward delivery and onset of the next trial rather than the ITI distribution. In practice the difference between the two is roughly the latency between the stimulus and the first lick and thus barely distinguishable at this scale. As the distribution indicates the probability of the next trial presentation as a function of time since the preceding reward delivery we refer to it as 'next-trial-probability'. (**C**) Same as inset in **B** averaged across all mice. Next-trial-probability was smoothed with a 20-point running average. (**D**) Next-trial-probability as a predictor of lick rate. The dotted lines indicate the 95% confidence bounds around the regression fit. Adjusted R^2 = 0.59. Although the next-trial-probability is a good predictor of changes in the average lick rate, the lick rate at the peak of the distribution is merely about a quarter higher than at its tails where next-trial-probability approaches zero. Furthermore, to put the average lick rates into perspective, note that mice tend to lick in bouts, typically consisting of two to six licks in very quick succession (see lick raster in **A**), and that, consequently, the lick rate exceeds the underlying bout rate by a factor of about four. (**E**) Same as **C** but with peri-catch trials binned into four quarters before averaging in order to illustrate changes in lick behavior across different stages of the experiment. (**F**) Same as **E** for all peri-catch trials during the initial training with a single-level stimulus. While the peri-catch trial lick rate profile changed substantially over the course of the initial training (**F**) and started to approximate the stimulus probability distribution towards the end of training, it remained broadly stable throughout the main experiment (**E**). In order to increase the statistical power for this analysis, we included data from several additional mice used in other projects. These additional mice received the same training and performed the same task, but differed from those in the main dataset in that they had a different genetic background and/or had been fitted with a cranial implant for cortical rather than midbrain imaging. N for panels **C-F** = 34 mice.

Video 1. Two-photon calcium imaging performed approximately 100 µm below the dorsal surface of the right IC of a GCaMP6f-reporter mouse (Ai95D) engaged in a sound detection task. GCaMP6f expression had been driven in corticorecipient IC neurons by injection of AAV1.hSyn.Cre.WPRE into the right auditory cortex. Video is played at twice the speed of acquisition and corresponds to the micrograph shown in Figure 4B.